Matrix representation of lateral soil movements: scaling and calibrating CE-DYNAM (v2) at a continental level

Arthur Nicolaus Fendrich[1,2,3], Philippe Ciais[2], Emanuele Lugato[1], Marco Carozzi[3], Bertrand Guenet[4], Pasquale Borrelli[5], Victoria Naipal[4], Matthew McGrath[2], Philippe Martin[3], and Panos Panagos[1]

[1]European Commission, Joint Research Centre, Sustainable Resources Directorate, Via E. Fermi 2749, I-21027 Ispra, Italy
[2]Laboratoire des Sciences du Climat et de l'Environnement, CEA-CNRS-UVSQ-UPSACLAY, Gif sur Yvette, France
[3]INRAE, UMR 1048 SAD-APT, 16 rue Claude Bernard, 75231, Paris, France
[4]LG-ENS (Laboratoire de géologie) - CNRS UMR 8538 - École normale supérieure, PSL University - IPSL, Paris, France
[5]Department of Science, Roma Tre University, 00146 Rome, Italy

Correspondence: Arthur Nicolaus Fendrich (arthur.fendrich@lsce.ipsl.fr; arthur.fendrich@ec.europa.eu)

Abstract. Promoting sustainable soil management is a possible option for achieving net-zero greenhouse gas emissions in the future. Several efforts in this area exist, and the application of spatially explicit models to anticipate the effect of possible actions on soils at a regional scale is widespread. Currently, models can simulate the impacts of changes on land cover, land management, and the climate on the soil carbon stocks. However, existing modeling tools do not incorporate the lateral transport and deposition of soil material, carbon and nutrients caused by soil erosion. The absence of these fluxes may lead to an oversimplified representation of the processes, which hinders, for example, a further understanding of how erosion has been affecting the soil carbon pools and nutrient through time. The sediment transport during deposition and the sediment loss to rivers create dependence among the simulation units, forming a cumulative effect through the territory. If, on the one hand, such a characteristic implies that calculations must be made for large geographic areas corresponding to hydrological units, on the other hand, it also can make models computationally expensive, given that erosion and redeposition processes must be modeled at high resolution and over long time scales. In this sense, the present work has a three-fold objective. First, we provide the development details to represent in matrix form a spatially explicit process-based model coupling sediment, carbon, and erosion, transport and deposition processes (ETD) of soil material in hillslopes and valley bottoms (i.e., the CE-DYNAM model). Second, we illustrate how the model can be calibrated and validated for Europe, where high-resolution datasets of the factors affecting erosion are available. Third, we presented the results for a depositional site, which is highly affected by incoming lateral fluxes from upstream lands. Our results showed that the benefits brought by the matrix approach to CE-DYNAM enabled the before precluded possibility of applying it to a continental scale. The calibration and validation procedures indicated: i) a close match between the erosion rates calculated and previous works on the literature at local and national scales; ii) the physical consistency of the parameters obtained from the data; and iii) the capacity of the model in predicting sediment discharge to rivers in locations observed and unobserved during its calibration (Model efficiency (ME) $= 0.603$, $R^2 = 0.666$; and ME $= 0.152$, $R^2 = 0.438$, respectively). The prediction of the carbon dynamics on a depositional site illustrated the model's ability to simulate the non-linear impact of ETD fluxes on the carbon cycle. We expect that our

work advances ETD models' description and facilitates its reproduction and incorporation in land surface models such as ORCHIDEE. We also hope that the patterns obtained in this work can guide future ETD models at a European scale.

1 Introduction

The adoption of more sustainable land management actions constitutes a critical alternative for mitigating climate change and sustaining food production (Roe et al., 2019). Soils constitute a vital carbon (C) pool for the world, storing 1500-2400 petagrams of carbon (PgC), more than the atmosphere (589 PgC) the surface ocean (900 PgC) together, and the way humans interact with soils affects how soils and the atmosphere interact, including the sequestration of carbon (Ciais et al., 2013). It is understood that even minor disturbances on soil pools can have significant impacts on the global C cycle: increases of 4‰ in global agricultural stocks, for example, could result in additional C sequestration of 2 to 3 PgC per year, which would contribute significantly to the Paris agreement targets (Guenet et al., 2020; Minasny et al., 2017; Soussana et al., 2019). Alternatives to rapidly increase the content of soil organic matter, and consequently the C sequestration from the atmosphere, include conservation agriculture (e.g., the retention of residues and zero or no-tillage) (Robert, 2001), agroforestry and afforestation. In the future, however, the projected population growth poses an increasing demand for food, feed, energy, and water, resulting in additional pressures that, if not properly dealt with, can even aggravate the problem (IPCC, 2019). An iconic example is the Southeastern Amazon forest, which has long been understood as a C sink, but after decades of deforestation, it is becoming a source of C to the atmosphere (Gatti et al., 2021; Nobre et al., 2016).

One of the possible strategies for evaluating the impacts of different alternatives on the C stocks is the use of numerical models that represent the physical, chemical, and biological processes of the soil-plant-atmosphere system, such as fixation by plants for biomass growth and the respiration by microorganisms (Gettelman and Rood, 2016). Models representing the interaction between soils and the atmospheric system allow the evaluation of how future climate change will impact soils and the opposite relationship. For example, land surface models (LSM) have allowed studies on different topics, such as assessing the impacts of climate change on crops, habitat, and water availability (Leng and Hall, 2019; Schewe et al., 2019; Hamaoui-Laguel et al., 2015; Bonan and Doney, 2018), evaluating strategies to achieve global environmental targets (Harper et al., 2018; Chang et al., 2021), forecasting future scenarios of change (Friedlingstein et al., 2006; Friedlingstein, 2015), among others. However, the implementation state of LSMs currently does not cover some relevant processes, such as lateral displacement of nutrients in the soil due to erosion, transport, and deposition (ETD) processes (Quine and van Oost, 2020a). ETD is argued to affect the carbon cycle dynamically during its occurrence by inducing lateral fluxes of C in the landscape and vertical fluxes between soil layers (Lal, 2003; Lugato et al., 2018), and their absence in LSMs leads to an oversimplified representation of the reality. The modeling complexity, along with the scarcity of empirical data for the phenomenon and the non-standardized nomenclature in the literature, hinder, for example, a further understanding of how erosion has been affecting the soil C pools through time (Lal, 2019; Lugato et al., 2018; Wang et al., 2017; van Oost et al., 2007).

Including the complex ETD-related processes into existing LSMs comes at the cost of increasing the inherent technical complexity of these mechanistic models, such as requiring massive amounts of codes, demanding costly computational resources,

and being hard to diagnose thoroughly (Lu et al., 2020). For example, even without ETD-related processes, existing LSMs are so complex with their detailed soil-vegetation-atmosphere feedbacks and multitude of spatial or temporal scales that simulations often must be performed repeatedly for hundreds or thousands of years until a stable condition is reached (Huang et al., 2018). In these cases, calculations can take hundreds of processor hours, and researchers often adopt less detailed or simplified processes to avoid prohibitively slow simulation times (Washington et al., 2008). Practically, such technical problems may hinder their operation by users, which are often individuals with different backgrounds and abilities. Since such problems can have an impact on model testing, validation, and ultimately acceptance by the scientific community, approaches to overcome them have been studied in the recent past. It is, for example, the case of the matrix approach, which consists of representing all carbon fluxes explicitly in matrix form (Luo et al., 2017), which has been reported to increase modularity, facilitate diagnostics, and accelerate spin-up calculations (Lu et al., 2020; Xia et al., 2012; Huang et al., 2017, 2018). For ETD-related processes, the incorporation and development of such approaches are advisable, encouraged and necessary to enable the complexity of representing the vertical and lateral dynamics of C and sediments on the landscape.

In this paper, we address the problem of scaling the calculations of CE-DYNAM, a hybrid empirical-mechanistic ETD model based on a physical emulator of the carbon cycle in soils (Naipal et al., 2020) to a continental scale. First, we describe the model formulation and show how the matrix approach leads to a sparse linear system, thus making calculations feasible. We expect our mathematical development of CE-DYNAM to facilitate its reproduction and incorporation in LSMs such as ORCHIDEE, DayCent, and others. We then calibrated the model for the study area (i.e., Europe) for the last 150 years using climate forcings with a monthly temporal and a 0.125° spatial resolution (approx. 12.5km at the Equator) using sediment concentration in rivers data collected on the field. Comparing the predictions against such observed values is important to evaluate the cumulative effect of all model assumptions, as well as its performance on catchments with different characteristics. Internal and external validation of the results is presented to show their consistency and physical realism. Finally, we exemplify the practical use of CE-DYNAM by presenting the results of the impact of ETD-related processes in a chosen depositional area in the territory. With the model in a matrix form, the calibration, and the pattern obtained at the depositional area, we expect to form the basis for future large-scale model applications.

2 Materials and Methods

2.1 Methodological proposal: the matrix approach

2.1.1 Definitions

The CE-DYNAM model (Naipal et al., 2020) consists of coupling erosion and transport modules to the soil carbon dynamics of any land surface model based on CENTURY (Parton et al., 1983, 1988). Typically, CE-DYNAM uses the Revised Universal Soil Loss Equation (RUSLE - Renard, 1997), approach adapted for predicting erosion at a large scale and a coarse spatial resolution, but any other existing option such as the LISEM model (de Roo et al., 1998) could be used. The transport module is a topography-based routing scheme, which uses the altitude (or an approximate digital elevation model) to distribute the

sediments and their corresponding organic carbon. The scheme is calibrated with field sediment discharge data to generate realistic values, and the elements are incorporated into the soil organic C dynamics as additional fluxes between pools beyond those initially present in the first-order kinetics of CENTURY (Naipal et al., 2015, 2016). As a remark, CE-DYNAM could be coupled to other carbon models as long as they adopt a first-order kinetics. Some advantages of the coupled approach of CE-DYNAM include the current incorporation of interactions such as the feedback between land use, climate, and erosion (Borrelli et al., 2020; Quine and van Oost, 2020b), and the potential for the future implementation of other components such as soil properties. Figure 1 presents a simplified representation of all fluxes of hillslopes and valley bottom soil pools in CE-DYNAM.

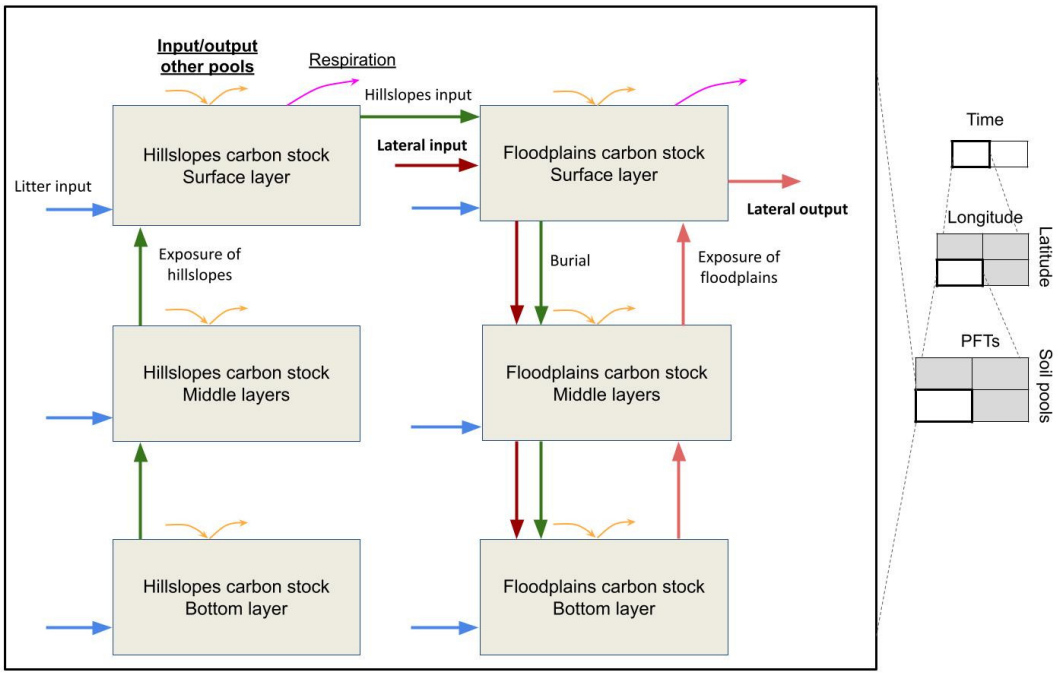

Figure 1. A simplified representation of all fluxes in CE-DYNAM. All colors represent the same flux (e.g., the blue arrow represents the input from litter). The example shown corresponds to a specific moment in time, spatial location, plant functional type (PFT), and soil pool. All fluxes with written descriptions are directly affected by the parameters to be calibrated (i.e., ρ_1, ρ_2 etc.), except for those with an underline. Fluxes whose description is in **bold** interact with one or more spatial locations, soil pools, or PFTs (right, gray squares)

CE-DYNAM has only been applied at a local scale, such as in the non-alpine region of the Rhine basin (whose total area equals 185.000 km^2) (Naipal et al., 2020). However, scaling the model for the continental scale, where the area can be tens of times larger than the application mentioned above, still faces practical implementation difficulties that we address in our current work. A careful evaluation of CE-DYNAM's original implementation allows the identification of three important remarks. First, from a computational point of view, the original implementation requires the storage of a large amount of data in the

computer's memory for its execution, which in practice becomes prohibitive as the geographical area or spatial resolution increases. Second, the original strategy is based on the subdivision of the problem in smaller and adjacent units - generally the sub-basins of a hydrographic basin. This procedure naturally restricts the ability to distribute the solution over different processing units and requires the continuous execution of additional steps of integration of all smaller units, which leads to a significant performance reduction. Third, the equilibrium calculation procedure of the original method consists of the successive iteration of the model, which can be very inefficient (Huang et al., 2018). Alternatives for these problems are more easily perceived when the models' mathematical notation is properly developed and stated.

Thus, to solve the problems above, we first clarify the notation to facilitate the comprehension of details and ensure reproducibility. We do so by adopting a general description and, when necessary, including examples based on ORCHIDEE (Krinner et al., 2005) to illustrate the concepts. The formulation accompanies Table 1, containing all input variables for the model, which helps clarification. The indices in Table 1 refer to five dimensions: the soil pool (c), the spatial location (x, interpreted here as point of a lattice X representing an area in the surface), the plant functional type (PFT) (p), the soil depth (d). Besides those dimensions, most variables also evolve in time (t). Some data sets are assumed constant on one or more dimensions during simulations: the geographic area of each cell, for example, varies in space but does not change according to the soil pools, PFTs, soil depth, nor time.

Mimicking the carbon dynamics of the LSM (in our case, ORCHIDEE) is the most important pillar of CE-DYNAM (Naipal et al., 2020). In general, we can represents the soil carbon pools setting of such LSMs with a set $\mathrm{C}_s = \{c_1, c_2, \ldots, c_n\}$. However, in comparison to the LSM in which it is based, CE-DYNAM makes additional assumptions to those described above. One of these assumptions is that the soil carbon pools are divided into two fractions: hillslopes and valley bottoms (i.e., $\mathrm{C}_s = \mathrm{C}_h \bigcup \mathrm{C}_v$), in such a way that the original number of soil carbon pools is twice the number of the LSMs. Such an assumption affects the original calculation depending on the fraction under consideration. For the hillslopes, calculations are modified by the inclusion of an extra flux proportional to the erosion predicted by a chosen model such as the RUSLE. For the valley bottoms, such a flux from hillslopes becomes a new input, and a new lateral dynamics of sediments across the landscape induced by the terrain slope (s_x) and the flow accumulation ($1/w_x$), is added. These lateral dynamics give rise to most computational challenges in CE-DYNAM since they make the stock in one simulation unit dependent on its neighbors.

Another assumption introduced by CE-DYNAM is a discretization of soil depth, which allows the evaluation of the vertical movement of carbon in layers even when the LSM does not. This is done by first setting $m = 3$ soil layers (that is, surface, middle and bottom layer) and then defining a set $\mathrm{D} = \{d_1, d_2, \cdots, d_m\}$ of soil layers. For example, if one let $d_1 = 10cm$, $d_2 = 20cm$ and $d_3 = 30cm$, then one is identifying the segment of soil from zero to $10cm$ as the surface, the segment from $10cm$ to $30cm$ as the middle layer and from $30cm$ to $60cm$ as the bottom layer. Throughout this text, we also use the symbol d_k, $k \in \{1, 2, \cdots, m\}$, to refer to the k-th layer. Then, the input from litter to soil pools are distributed along D to form ${I^*}^j_{x,p_l,d}(t)$. We describe the vertical discretization in subsubsection 2.1.2.

Because the LSM used in this work is based on CENTURY, carbon pool kinetics will always follow a first-order differential equation. Furthermore, soil carbon is divided into three pools (active, slow, passive) with different turnover rates that vary with temperature, moisture, clay content, and other modifiers (e.g., tillage) (Camino-Serrano et al., 2018). The set of $v = 15$ plant

Table 1. The external input variables for CE-DYNAM calculation.

Notation	Description	Source
$u_{x,p_l}(t)$	The percentage of each plant functional type (PFT) in each cell. $0 < u_{x,p_l}(t) < 1$, so one cell cannot be more than 100% covered by a PFT; and $\sum_l u_{x,p_l}(t) = 1$	This information comes from the land surface model.
a_x	The geographic area (km^2) of each cell	Derived from each cell's bounding box.
b_{x,d_k}	The bulk density (g/cm^3).	Several potential sources are available, for example the Global Soil Dataset for Earth System Modeling (≈1km) (Shangguan et al., 2014) and SoilGrids (250m) (Poggio et al., 2021).
α_x	The depth to bedrock (cm)	SoilGrids (250m) (Poggio et al., 2021)
ν_{x,d_k}	The soil organic carbon stock (tonnes)	Derived from SoilGrids (250m) (Poggio et al., 2021)
$\kappa^{i,j}_{x,p_l}(t)$	The turnover rates from carbon pool c_i to carbon pool c_j (1/day).	These rates are calculated from the output of the land surface model.
$\rho^{i}_{x,p_l}(t)$	The respiration rates of carbon pool c_i (1/day).	Idem as above.
$I^{j}_{x,p_l}(t)$	The input from litter pools to carbon pool c_j (gC/(m^2.day)).	Idem as above.
$e_{x,p_l}(t)$	The average erosion rate (tonnes/(ha.day))	Calculated from any erosion model such as the Universal Soil Loss Equation, the Water Erosion Prediction Project etc.
s_x	The terrain slope (degrees).	Derived from any digital elevation model such as from the Shuttle Radar Topography Mission (Farr et al., 2007)
$1/w_x$	The adimensional flow accumulation (i.e., the cumulative number of upstream drainage cells).	Idem as above, preferably from the same source as the terrain dataset.
h_x	The fraction of each cell belonging to hillslopes. $(1 - h_x)$ is the fraction of valley bottoms.	Pelletier et al. (2016)
l_x	The river width (m)	Derived from HydroSheds (Lehner et al., 2008)

functional types used to represent land cover in the model is denoted here as $P = \{p_1, p_2, \cdots, p_v\}$. Then, for a fixed layer $d_k \in D$, a fixed lattice point $x \in X$, a fixed PFT $p_l \in P$, a fixed pool $c_i \in C_s$ and a fixed time t we let $S^i_{x,p_l,d_k}(t)$ denote its carbon stock.

The formulas for the CE-DYNAM rates are detailed in later sections of the text. However, we can essentially represent how the model evolves in time with Equation 1. While such a representation omits most model dimensions, it's useful to clarify its dynamics as that of a linear and non-autonomous model (Sierra et al., 2018, Table 1). As we will describe in the following subsections, the coupling of erosion-related processes will always respect this general structure, with the changes consisting of modifications to each of its elements according to the particular case.

$$\frac{dS}{dt} = \mathrm{I}(t) - k(t) \cdot S(t) \tag{1}$$

with $S(t)$ denoting the carbon stock at time t in the pool, $\mathrm{I}(t)$ denoting all the pool's input, and $k(t)$ denoting the output rates. In the equilibrium calculation, the model was iterated several times over the period 1860-1869 until convergence to the pullback attracting trajectory (Sierra et al., 2018). In the transient period, all the elements on the right-part of the equation will be known and dS/dt calculated will correspond to the increment in carbon stocks at each time step. Essentially, we are interested in evaluating how the carbon stocks $S(t)$ change over the transient period. Through the rest of the text, we frequently refer to Equation 1 as the basis to form the carbon budget in all cases.

In the matrix approach, we discretize Equation 1 and represent all fluxes between pools of as a linear system. Hypothetically, if no fluxes between pools existed, we would have

$$S(t + \Delta t) = S(t) + I(t) \cdot \Delta t - A(t)S(t) \cdot \Delta t, \tag{2}$$

where $S(t) = \left[S^i_{x,p_l,d_k}(t)\right]_{\substack{x\in X\\ l\in[v]\\ k\in[m]\\ i\in[n]}} \in \mathbb{R}^{|X|\times v\times m\times n}$, $I(t) = \left[I^i_{x,p_l,d_k}(t)\right]_{\substack{x\in X\\ l\in[v]\\ k\in[m]\\ i\in[n]}} \in \mathbb{R}^{|X|\times v\times m\times n}$ and $A(t)$ is a diagonal matrix with diagonal $\left[\kappa^{i,i}_{x,p_l,d_k}(t)\right]_{\substack{x\in X\\ l\in[v]\\ k\in[m]\\ i\in[n]}} \in \mathbb{R}^{|X|\times v\times m\times n}$.

However, interactions tend to be complex in more general situations. The following sections show that the routing scheme for valley bottoms creates a dependence between pools of different grid cells, PFTs, and soil layers. While such a property replaces several off-diagonal zero elements of $A(t)$ by non-zero rates, it still preserves the inherently sparse structure of $A(t)$.

Next, we detail how the elements of $A(t)$ and $I(t)$ can be calculated. For simplicity, we exemplify with the first timestep of the equilibrium period ($t = t_0$), but calculations are analogous for all timesteps.

2.1.2 Vertical discretization

As mentioned in subsubsection 2.1.1, CE-DYNAM vertically discretizes the soil, which has a direct impact on the respiration, erosion, and turnover rates of the original LSM. An exponential increase of the profile depth is assumed, so each soil layer thickness in the discretization profile is calculated from the depth to bedrock, α_x, using two real-valued parameters γ_1 and r:

$$d_{m-k+1} = \int_{z=(k-1)/m}^{z=k/m} \alpha_x \cdot \exp(\gamma_1 + r \cdot z)\mathrm{d}z = \frac{\alpha_x}{r} \cdot \left[\exp\left(\gamma_1 + r \cdot \frac{k}{m}\right) - \exp\left(\gamma_1 + r \cdot \frac{k-1}{m}\right)\right] \; \forall k = 1, 2, \cdots, m. \quad (3)$$

For any choice of γ_1, the parameter r is calculated by constraining the sum of all vertical layers to match the total distance to bedrock. By using the general properties of definite integrals, it is possible to show that it can be analytically calculated with the closed-form solution

$$r = -\exp(\gamma_1) - \mathrm{W}\left[-\exp(\gamma_1 - \exp(\gamma_1))\right], \quad (4)$$

where $\mathrm{W}(\cdot)$ representing the Lambert W function (see Corless et al., 1996). The example notation of Equation 3 and Equation 4 shows an important property of the vertical discretization scheme: the γ_1 parameter depends solely on the soil discretization setting, which is assumed to be identical for all cells in CE-DYNAM. For this reason, there is a single γ_1 value independent of all factors being different (e.g., the spatial location, the PFT or the variable to be discretized). Besides, this property also means that the vertical discretization is not scale-invariant, and thus the depth scheme must be defined with extra care. In Figure 2, we show how a possible vertical profile of depth equal to 2m varies with γ_1: for values closer to zero (left), the profile tends towards a flat one, while for larger values (right), the model tends to calculate a smaller surface layer. The realistic choice of γ_1 must come from the model calibration procedure.

In the carbon simulation, the input from litter to soil pools is also vertically discretized. This is done by multiplying the original quantity (i.e., $I^j_{x,p_l}(t)$) by the percentage of soil organic carbon in each soil layer (Poggio et al., 2021).

$$I^{*j}_{x,p_l,d_k}(t) = I^j_{x,p_l}(t) \cdot \frac{\nu_{x,d_k}}{\sum_d \nu_{x,d}}, \quad (5)$$

For the erosion rates, the vertical discretization is assumed inversely proportional to the mass of soil in each layer. Since not all the carbon eroded in hillslopes goes to valley bottoms, the term is multiplied by a fraction from zero to one, assumed to vary with terrain slope and land cover. A different curve is assumed for forests, croplands, and grasslands, and their calibration is made using field observations.

$$\lambda_{x,p_l,d_k}(t) = \underbrace{\frac{\overbrace{e_{x,p_l}(t)}^{\text{RUSLE rate}}}{\underbrace{b_{x,d_k} \cdot d_k \cdot h_{x,p_l} \cdot a_x}_{\text{Total mass of soil}}}}_{} \cdot \overbrace{\frac{1}{1 + \exp(g_f(s_x))}}^{\text{\% of erosion that goes to valley bottoms}}, \quad (6)$$

with the multiplication by h_{x,p_l} varying for hillslopes and valley bottoms according to their fractions, and $g_f(s_x)$ being the weighted sum of the different smoothing function for forests, croplands, and grasslands multiplied by their corresponding land cover fractions. Although not explicit in the notation, such a function also varies on time since land cover varies each year.

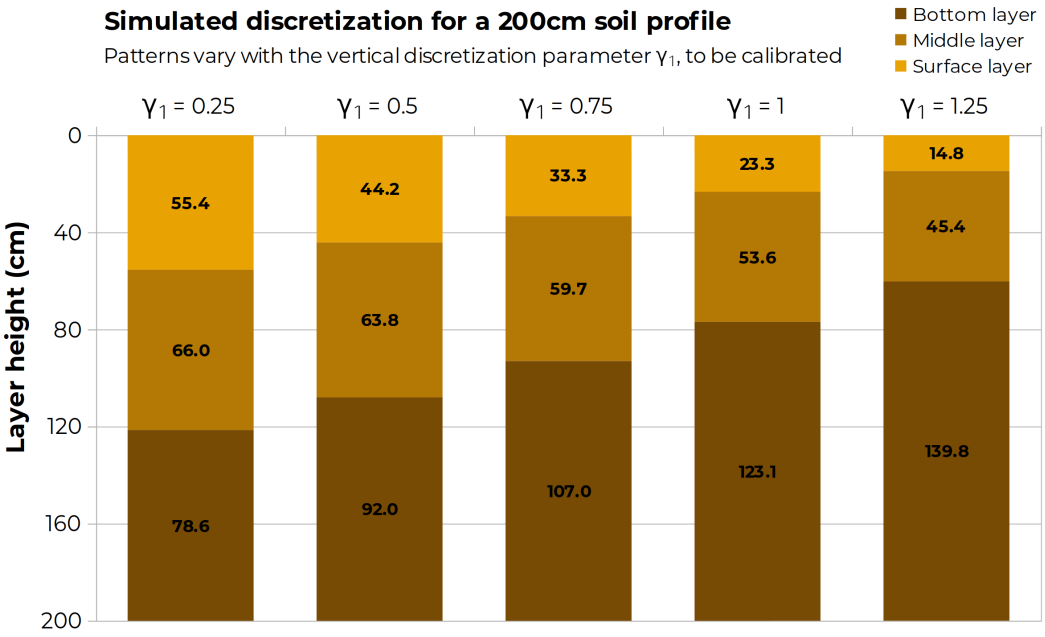

Figure 2. Possible options for the vertical discretization parameter in CE-DYNAM. The vertical axis shows the layer heights in centimeters, and the horizontal axis shows some possible γ_1 values.

2.1.3 Fluxes: hillslopes soil carbon pools

Bottom soil layer: d_m

We describe the carbon dynamics in hillslopes in terms of three general pools $c_1, c_2, c_3 \in \mathrm{C}_h$, which can be interpreted in terms of the active, slow, and passive soil pools of ORCHIDEE. For the deepest soil layer, the rearrangement of Equation 1 leads to the following equations for c_1, c_2 and c_3, respectively:

$$\frac{dS^1_{x,p_l,d_m}(t_0)}{dt} = \left(\overbrace{\sum_{c_i \in C_l} I^{*1}_{x,p_l,d_m}(t_0)}^{\text{Input: litter pools}} + \overbrace{\kappa^{2,1}_{x,p_l}(t_0) \cdot S^2_{x,p_l,d_m}(t_0)}^{\text{Input: } c_2 \text{ pool}} + \overbrace{\kappa^{3,1}_{x,p_l}(t_0) \cdot S^3_{x,p_l,d_m}(t_0)}^{\text{Input: } c_3 \text{ pool}} \right)$$

$$- \left(\overbrace{\rho_{x,p_l}(t_0)^1}^{\text{Respiration rate}} + \overbrace{\kappa^{1,2}_{x,p_l}(t_0)}^{\text{Output: } c_2 \text{ pool}} + \overbrace{\kappa^{1,3}_{x,p_l}(t_0)}^{\text{Output: } c_3 \text{ pool}} + \overbrace{\lambda_{x,p_l,d_m}(t_0)}^{\text{Output: erosion } b \rightarrow t} \right) \cdot \overbrace{S^1_{x,p_l,d_m}}^{c_1 \text{ stock}} \quad (7)$$

$$\frac{dS^2_{x,p_l,d_m}(t_0)}{dt} = \left(\sum_{c_i \in C_l} I^{*2}_{x,p_l,d_m}(t_0) + \kappa^{1,2}_{x,p_l}(t_0) \cdot S^1_{x,p_l,d_m} + \kappa^{3,2}_{x,p_l}(t_0) \cdot S^3_{x,p_l,d_m}(t_0) \right)$$

$$- \left(\rho^2_{x,p_l}(t_0) + \kappa^{2,1}_{x,p_l}(t_0) + \kappa^{2,3}_{x,p_l}(t_0) + \lambda_{x,p_l,d_m}(t_0) \right) \cdot S^2_{x,p_l,d_m}(t_0) \quad (8)$$

$$\frac{dS^3_{x,p_l,d_m}(t_0)}{dt} = \left(\sum_{c_i \in C_l} I^{*3}_{x,p_l,d_m}(t_0) + \kappa^{1,3}_{x,p_l}(t_0) \cdot S^1_{x,p_l,d_m} + \kappa^{2,3}_{x,p_l}(t_0) \cdot S^2_{x,p_l,d_m}(t_0) \right)$$

$$- \left(\rho^3_{x,p_l}(t_0) + \kappa^{3,1}_{x,p_l}(t_0) + \kappa^{3,2}_{x,p_l}(t_0) + \lambda_{x,p_l,d_m}(t_0) \right) \cdot S^3_{x,p_l,d_m}(t_0) \quad (9)$$

Since CE-DYNAM does not affect litter pools, all quantities on the equations above should be known, except the three hillslope soil carbon pools in equilibrium calculation.

Middle and top soil layers

In hillslopes, the structure for middle and top soil layers will be identical as for bottom layers, except for the $b \rightarrow t$ loss from the layers below (i.e., the fourth term of Equation 7), which becomes a new input to the layers above. This results in an additional input equal to $\lambda_{x,p_l,d_{k+1}}(t_0) \cdot S^j_{x,p_l,d_{k+1}}(t_0)$, in case of pool c_j and depth d_k. One important final remark is that, for the top soil layer, the interpretation of the "Output: erosion b $\rightarrow$ t" rate becomes "Output: erosion hillslopes $\rightarrow$ valley bottoms".

2.1.4 Fluxes: valley bottoms soil carbon pools

Preliminary assumptions

In the hillslopes soil carbon pools described above, the movement of C was spatially static, which means that all calculations were performed within the same spatial unit (i.e., grid cell). However, the physical definition of valley bottoms extends the movement to other cells since connected areas exchange sediments and C according to the terrain and land cover configuration. This characteristic is incorporated into the CE-DYNAM model by defining a routing scheme that transports sediments along the landscape.

To represent the lateral transport, a new rate τ_x derived from the sediment residence time is added. Its calculation is performed as:

$$\overbrace{\tau_x}^{\text{Sediment rate}} = \underbrace{\frac{1}{g_\tau(1/w_x)}}_{\text{Residence time}} \tag{10}$$

with $g_\tau(1/w_x)$ representing a smoothing function between the sediment residence time and the flow accumulation (i.e., upstream area), to be calibrated from the observations. In this work, we adopted 3rd degree B-Spline to represent all smoothing functions. Besides, the flow accumulation information is also used in the routing scheme to generate an approximated digital elevation model, w_x. Such an approximation is used instead of the original terrain to ensure a hydrologically consistent topography for the lateral movements.

Also, let $\mathrm{P}_x^+(t)$ be the number of non-zero PFTs in cell x at time t and $\mathrm{Q}(x)$ be the set of queen neighbors (Figure 3) (Quinn et al., 1991) of a given cell x formed as:

$$\mathrm{Q}(x) = \{y : y - x \in \{-1,0,1\} \times \{-1,0,1\}, y \neq x\}$$

$x+(-1,1)$	$x+(0,1)$	$x+(1,1)$
$x+(-1,0)$	x	$x+(1,0)$
$x+(-1,-1)$	$x+(0,-1)$	$x+(1,-1)$

Figure 3. Queen neighbor setting used for the routing scheme. The center cell (red) is x.

With these definitions, the routing scheme for a given cell consists of two elements incorporated into its C balance. First, at the surface depth, d_0, there is loss from the cell to its neighbors, but some definitions are necessary to dictate how the process occurs:

1. The routing scheme works only within the same carbon pool. For example, the *active carbon* routed from one cell is added exclusively to the *active carbon pool* of its neighbor cells.
2. The C from one PFT in the source cell is transferred equally to all non-zero PFTs of the target cell.
3. The bare soil PFT (conventionally denoted here by p_0) loses and gains no C on the routing scheme.

The rate of routed C from a PFT p_r of the source cell x to a PFT p_l of the target cell y can then be calculated as:

$$\overbrace{\theta_{[\underbrace{x}_{\text{Source}},\underbrace{y}_{\text{Target}}]}}^{\text{Lateral transfer rate}} = \overbrace{\mathbb{1}_{(w_y<w_x)}}^{\text{Indicator function}} \cdot \overbrace{\frac{w_x - w_y}{||x-y||_2}}^{\text{Slope: rise/run}} \tag{11}$$

$$\overbrace{\zeta_{x,p_r,y,p_l}(t)}^{\text{Rate of routed carbon}} = \overbrace{\mathbb{1}_{(p_l\neq p_0,p_r\neq p_0)}}^{\text{Indicator}} \cdot \overbrace{\tau_x}^{\text{Sediment rate}} \cdot \overbrace{\frac{\theta_{x,y}}{\sum_{y\in Q(x)}\theta_{x,y}}}^{\text{Local \% of lateral transfer}} \cdot \overbrace{\frac{u_{y,p_l}(t)}{\sum_{s=1}^{v} u_{y,p_s}(t)}}^{\text{Local \% of target PFT}} \tag{12}$$

where the indicator function, $\mathbb{1}$, equals to one when the condition is met or zero otherwise. Together, Equation 11 and Equation 12 result in the important remark: the total loss of C in PFT $p_r \neq p_0$ of the source cell is equal to τ_x times the corresponding C stock at the surface, which varies according to the pool under consideration (for example, $S^1_{x,p_r,d_0}(t_0)$ for pool c_1). Also, the flux is equal to zero for the remaining case of $p_r = p_0$ since the bare soil does not participate in the routing scheme. At the surface, the equilibrium value of C stock in one cell and PFT will depend on the equilibrium value of C stock in all the PFTs of all its neighbors. This property of the routing scheme is essential and makes several zero off-diagonal elements be represented as rates from/to different grid cells, PFTs or soi layers.

Besides, despite affecting more directly the soil surface layer, the routing scheme is also assumed to affect the vertical movement of C earlier described in subsubsection 2.1.3 for the case of hillslopes. The same total rate routed from one PFT to the neighbors also moves through the layers, from the bottom to the top ($b \rightarrow t$) (i.e., subsoil exposure). In the other way ($t \rightarrow$b), the rate received from the neighbors is transmitted vertically from each layer to the layer below (i.e., burial). The only exception is naturally d_m, which has no layers below. Such input rate to p_l can be denoted as: $\sum_{y\in Q(x)}\sum_{r=1}^{v}\zeta_{y,p_r,x,p_l}(t)$.

Top soil layer: d_0

The equations for the C dynamics in valley bottoms can be obtained by putting the new fluxes along with the other ones from the original LSM. This implicitly assumes that litter input and PFT in valley bottoms are the same than in the standard LSM. Again, we make this section using a general notation of $c_1, c_2, c_3 \in \mathrm{C}_h$ and its respectively correspondent pools $c_4, c_5, c_6 \in \mathrm{C}_v$. For example, if c_1 is the hillslope soil active carbon pool, then c_4 is the valley bottoms soil active carbon pool. Below, we describe the fluxes for PFT p_l of pool c_4 using element-wise notation. For the topsoil layer, d_0, we have input from below but not from above, and also have inputs from some neighbor cells via the routing scheme and losses for other neighbors for the same reason.

$$\frac{dS^4_{x,p_l,d_0}(t_0)}{dt} = \Bigg(\overbrace{\sum_{c_i \in C_l} {I^*}^4_{x,p_l,d_0}(t_0)}^{\text{Input: litter pools}} + \overbrace{\kappa^{6,4}_{x,p_l}(t_0) \cdot S^6_{x,p_l,d_0}(t_0)}^{\text{Input: } c_6 \text{ pool}} + \overbrace{\kappa^{5,4}_{x,p_l}(t_0) \cdot S^5_{x,p_l,d_0}(t_0)}^{\text{Input: } c_5 \text{ pool}}$$

$$+ \overbrace{\lambda_{x,p_l,d_0}(t_0) \cdot S^1_{x,p_l,d_0}(t_0)}^{\text{Input: hillslopes}} + \overbrace{\sum_{y \in Q(x)} P^+_y(t_0) \cdot \tau_x \cdot S^4_{x,p_l,d_1}(t_0)}^{\text{Input: vertical flow } b \to t}$$

$$+ \overbrace{\sum_{y \in Q(x)} \sum\nolimits_{r=1}^{v} \zeta_{y,p_r,x,p_l}(t_0) \cdot S^4_{y,p_r,d_0}(t_0)}^{\text{Input: routing scheme}} \Bigg)$$

$$- \Bigg(\overbrace{\rho^4_{x,p_l}(t_0)}^{\text{Respiration rate}} + \overbrace{\kappa^{4,5}_{x,p_l}(t_0)}^{\text{Output: } c_5 \text{ pool}} + \overbrace{\kappa^{4,6}_{x,p_l}(t_0)}^{\text{Output: } c_6 \text{ pool}} + \overbrace{\sum_{y \in Q(x)} P^+_y(t_0) \cdot \tau_x}^{\text{Output: routing scheme + extra respiration}}$$

$$+ \overbrace{\lambda_{x,p_l,d_0}(t_0)}^{\text{Output: erosion } t \to b} + \overbrace{\sum_{y \in Q(x)} \sum\nolimits_{r=1}^{v} \zeta_{y,p_r,x,p_l}(t_0)}^{\text{Output: vertical flow } t \to b} \Bigg) \cdot \overbrace{S^4_{x,p_l,d_0}(t_0)}^{c_4 \text{ stock}} \tag{13}$$

For the other pools c_5 and c_6, the equations are analogous.

Middle layers

The routing scheme for valley bottoms also affects the middle layers with its vertical components. For having layers above and below, such layers have fluxes in both directions. For a PFT p_l of pool c_4, the equation for d_k, $0 < k < m$, is:

$$\frac{dS^4_{x,p_l,d_k}(t_0)}{dt} = \Bigg(\overbrace{\sum_{c_i \in C_l} I^{*4}_{x,p_l,d_k}(t_0)}^{\text{Input: litter pools}} + \overbrace{\kappa^{6,4}_{x,p_l}(t_0) \cdot S^6_{x,p_l,d_k}(t_0)}^{\text{Input: } c_6 \text{ pool}} + \overbrace{\kappa^{5,4}_{x,p_l}(t_0) \cdot S^5_{x,p_l,d_k}(t_0)}^{\text{Input: } c_5 \text{ pool}}$$
$$+ \left[\overbrace{\lambda_{x,p_l,d_{k-1}}(t_0)}^{\text{Input: erosion } t \to b} + \overbrace{\sum_{y \in Q(x)} \sum\nolimits_{r=1}^{v} \zeta_{y,p_r,x,p_l}(t_0)}^{\text{Input: vertical flow } t \to b} \right] \cdot S^4_{x,p_l,d_{k-1}}(t_0)$$
$$+ \overbrace{\sum_{y \in Q(x)} P^+_y(t_0) \cdot \tau_x \cdot S^4_{x,p_l,d_{k+1}}(t_0)}^{\text{Input: vertical flow } b \to t} \Bigg)$$
$$- \Bigg(\overbrace{\rho^4_{x,p_l}(t_0)}^{\text{Respiration rate}} + \overbrace{\kappa^{4,5}_{x,p_l}(t_0)}^{\text{Output: } c_5 \text{ pool}} + \overbrace{\kappa^{4,6}_{x,p_l}(t_0)}^{\text{Output: } c_6 \text{ pool}} + \overbrace{\sum_{y \in Q(x)} \sum\nolimits_{r=1}^{v} \zeta_{y,p_r,x,p_l}(t_0)}^{\text{Output: vertical flow } t \to b}$$
$$+ \overbrace{\lambda_{x,p_l,d_k}(t_0)}^{\text{Output: erosion } t \to b} + \overbrace{\sum_{y \in Q(x)} P^+_y(t_0) \cdot \tau_x}^{\text{Output: vertical flow } b \to t} \Bigg) \cdot \overbrace{S^4_{x,p_l,d_k}(t_0)}^{c_4 \text{ stock}} \tag{14}$$

Bottom soil layer: d_m

Finally, for the bottom soil layer, the equation is identical as Equation 14, the exception being the inexistence of $b \to t$ input or $t \to b$ output rates, since there are no bottom layers. In this case, for a given PFT p_l of pool c_4, we have:

$$\frac{dS^4_{x,p_l,d_m}(t_0)}{dt} = \Bigg(\overbrace{\sum_{c_i \in C_l} I^{*4}_{x,p_l,d_m}(t_0)}^{\text{Input: litter pools}} + \overbrace{\kappa^{6,4}_{x,p_l}(t_0) \cdot S^6_{x,p_l,d_m}(t_0)}^{\text{Input: } c_6 \text{ pool}} + \overbrace{\kappa^{5,4}_{x,p_l}(t_0) \cdot S^5_{x,p_l,d_m}(t_0)}^{\text{Input: } c_5 \text{ pool}}$$
$$+ \left[\overbrace{\lambda_{x,p_l,d_{m-1}}(t_0)}^{\text{Input: erosion } t \to b} + \overbrace{\sum_{y \in Q(x)} \sum\nolimits_{r=1}^{v} \zeta_{y,p_r,x,p_l}(t_0)}^{\text{Input: vertical flow } t \to b} \right] \cdot S^4_{x,p_l,d_{m-1}}(t_0) \Bigg)$$
$$- \Bigg(\overbrace{\rho^4_{x,p_l}(t_0)}^{\text{Respiration rate}} + \overbrace{\kappa^{4,5}_{x,p_l}(t_0)}^{\text{Output: } c_5 \text{ pool}} + \overbrace{\kappa^{4,6}_{x,p_l}(t_0)}^{\text{Output: } c_6 \text{ pool}} + \overbrace{\sum_{y \in Q(x)} P^+_y(t_0) \cdot \tau_x}^{\text{Output: vertical flow } b \to t} \Bigg) \cdot \overbrace{S^4_{x,p_l,d_m}(t_0)}^{c_4 \text{ stock}} \tag{15}$$

2.2 Study area

In this work, the study area comprises the European Union member states (EU27), plus Switzerland, the United Kingdom, and the Balkan states (i.e., Albania, Bosnia and Herzegovina, Kosovo, Montenegro, North Macedonia and Serbia). The EU27 is

a political and economic block of 27 countries, covering 410 million hectares - larger than the seventh-largest country in the world (India) - and 447 million inhabitants. Switzerland, the United Kingdom, and the Balkan States were included for being spatially adjacent territories. The food and farming sector of EU27 used 156.7 million hectares of land (i.e., 38.2% of the total area) for agricultural production in 2016 and currently provides nearly 40 million jobs (i.e., 9.75% of the total population) (Statistical Office of the European Union, 2020; European Union, 2021).

EU27 has been promoting changes to shift its agriculture towards more sustainable practices. In 2019, for example, the European Commission proposed the European Green Deal, a growth strategy for the continent that proposes environmental targets, including climate neutrality by 2050. Some of the targets include increasing the share of organic farming from 8.5% of the total agricultural land to 30% by 2030 and increasing tree cover by planting 3 billion additional trees also by 2030 (European Commission, 2021). Such actions come as an anticipated response to projections of future environmental conditions. For example, the projected patterns of rainfall erosivity for the future indicate an increase in 81% of the European territory by 2050 (Panagos et al., 2017), which will consequently affect soils, a very relevant natural resource for the achievement of the European Green Deal's goals (Montanarella and Panagos, 2021).

2.2.1 Input data: LSM emulator and erosion rates

The first step to running CE-DYNAM is to build a standalone version of the soil carbon dynamics of an existing LSM, i.e., an emulator. Such procedure is done by carefully analyzing and modifying the source code of the original LSM to allow the export of all necessary variables for reproducing calculations externally. In this work, we ran ORCHIDEE, a process-based model that simulates vegetation, energy, water, and carbon fluxes (Krinner et al., 2005), with the following settings: i) version: ORCHIDEE 2.2; ii) time step and range: daily, from 01/01/1860 to 31/12/2018; ii) climate: monthly forcings at a 0.125° spatial resolution from the VERIFY project (see https://verify.lsce.ipsl.fr/index.php/presentation); iii) land cover: annual forcing - derived from the ESA CCI Land Cover dataset (European Spatial Agency, 2021; LSCE, 2021).

For the calculation of erosion rates, we applied the well-known Revised Universal Soil Loss Equation (RUSLE) model, using the values recently developed by the European Commission specifically for our study area (Panagos et al., 2015e). For a given year (y) and month (m), monthly erosion rate (E), in $t/(ha \cdot year \cdot PFT)$ was calculated as:

$$E(y,m) = R(y,m) \cdot K \cdot C(y) \cdot LS \cdot P \tag{16}$$

with $R(y,m)$ being the rainfall erosivity factor[1] in $MJ \cdot mm \cdot ha^{-1} \cdot h^{-1} \cdot yr^{-1}$, K being the soil erodibility factor[2] in $t \cdot ha \cdot h \cdot ha^{-1} \cdot MJ^{-1} \cdot mm^{-1}$, $C(y)$ being the dimensionless land cover and management factor[3], LS being the dimensionless slope

[1] It represents the "kinetic energy of raindrop's impact and the rate of associated runoff" (Panagos et al., 2015a; Wischmeier et al., 1978)

[2] It "represents an integrated annual value of the soil profile reaction to the process of soil detachment and transport by raindrops and surface flow" (Panagos et al., 2014; Renard, 1997)

[3] It "accounts for how land cover, crops and crop management cause soil loss to vary from those losses occurring in bare fallow areas" (Panagos et al., 2015c; Kinnell, 2010)

length and steepness factor[4], and P being the dimensionless support practices factor[5]. When collapsing the PFT dimension for the calculation of annual or monthly averages, $E(y,m)$ was multiplied by the corresponding land cover fraction p_i for PFT i (Table 1). All the data was aligned and processed on a 0.125° grid.

As seen in Equation 16, factors K, LS and P were assumed constant for the whole period 1860 - 2018, while $R(y,m)$ varies per month and $C(y)$ varies annually. The source of K is the extrapolated version of Panagos et al. (2014) including stoniness, LS comes from the completely harmonized version of Panagos et al. (2015b) for the whole study area, and P comes from the database provided by Panagos et al. (2015d). The first and the second factors cover the whole study area originally, but the third does not, so an additional assumption was added: in places where P was not available (i.e., Switzerland and the Balkan states), it was assumed to be equal to 1. According to the authors mentioned above, K and P were derived from field survey data caried out in 2009 and 2012, respectively.

For C, we used the spatial dataset of Panagos et al. (2015c), but an additional procedure was made to minimize the differences arising from the mismatch in the land cover classes definition and spatial resolution. Such a procedure consisted of fitting a linear regression model to the upscaled version of the original C factor using the target land cover classes as explanatory variables (i.e., $C = \sum_i \beta_i \overline{p}_i + \epsilon, \quad \epsilon \sim \mathrm{N}(0, \sigma^2)$). An intercept term was intentionally not added to the linear regression, and $\overline{p_i}$ is the average land cover from the period 2010-2018, approximately the period of data collection of Panagos et al. (2015c).

The rainfall erosivity also demanded an extra processing step. The main source for calculations was the monthly erosivity derived and provided by Ballabio et al. (2017). To extrapolate for the past, we assumed a constant erosivity density for the whole simulation period, 1860-2018. That was made by calculating:

$$R(y,m) = r(y,m) \cdot \frac{R^*(m)}{\overline{r}(m)}$$

with $R^*(m)$ being the original monthly erosivity data set upscaled to a 0.125° spatial resolution, $\overline{r}(m)$ being the average monthly precipitation of the period 2010-2018 (roughly the same data collection period of Ballabio et al. (2017)), and $r(y,m)$ being the monthly precipitation for the month m of year y.

2.2.2 Calibration and validation

Calibration

Calibrating CE-DYNAM means ensuring that the values predicted by the routing scheme introduced are realistic and consistent with field observations. To do so, we made an exact copy of the model described in subsubsection 2.1.3 and subsubsection 2.1.4, but replacing the carbon quantities with sediment quantities. Then, we used as field data the information of total suspended solids and river discharge from the GEMStat database (United Nations Environment Programme, 2018) for the whole Europe. We adopted a squared error cost function between the model predictions and the observations. Because the calculation of

[4]It describes "the effect of topography on soil erosion" (Panagos et al., 2015b)

[5]It "accounts for control practices that reduce the erosion potential of runoff by their influence on drainage patterns, runoff concentration, runoff velocity and hydraulic forces exerted by the runoff on the soil surface" (Panagos et al., 2015d; Renard et al., 1991)

analytical derivatives of the cost function with respect to the parameters is hard in our case, minimization was performed using the NEWUOA solver (Powell, 2006, 2008) with early stopping to prevent overfitting.

Like most optimization methods, NEWUOA requires several evaluations of the cost function, which is computationally expensive in our case. For this reason, we calibrated the model using annual averages instead of monthly inputs to accelerate calculations. We also pre-processed our observations by first aggregating annually the total of 10,552 instantaneous observations available, which resulted in 391 annual median values for 40 rainfall stations distributed across Europe from 1979 to 2003. Then, we calculated the 5-year moving averages of the median annual values to simultaneously smooth extreme values from floods that are not modeled in CE-DYNAM and remove stations with a small number of observations. The final dataset contained 241 observations in 30 stations, whose contributing areas covered nearly one-fourth (23.34%) of the study area. For each set of parameters, we calculated the predicted sediment stock in the river fraction of the cell (from variable l_x, see Table 1), and the objective function adopted was the squared error between this quantity and the product between the total suspended sediments observed and the water volume in a day (derived from the instantaneous discharge). As in similar works such as Borrelli et al. (2018), the model was assessed using the Nash-Sucliffe model efficiency (ME) coefficient (Nash and Sutcliffe, 1970), and the coefficient of determination (R^2) as defined by Everitt and Skrondal (2010).

Validation

The hillslope erosion rates were externally validated by comparing our estimates with some field observations and modeled values in the literature. We used the compilation of observations by Cerdan et al. (2010) in two ways: i) we aggregated our and their land cover classes into four common categories (i.e., croplands, grasslands, forest, and bare soil), and compared the distribution of our calculations with their reported point estimates; ii) we compared our country averages with their extrapolated calculations for the whole Europe. We also compared our erosion values to the compilation of local-scale field observations from different sources reported by Panagos et al. (2020) and modeled country averages of (Panagos et al., 2015e) to evaluate the model behavior at a local and regional scale, respectively.

The calibration of the lateral movements on the model was validated both internally and externally. The model's internal consistency was checked by comparing the physical quantities obtained empirically by the calibration procedure with the results previously obtained in the literature. We checked the model's ability to predict the sediment concentrations in places unobserved during the calibration process. For this purpose, the 30 rainfall stations of the final dataset were divided between 24 stations for calibration - i.e., 80% observed by the model - and six stations for validation - i.e., 20% unobserved by the model.

2.3 Simulations

In order to evaluate the behavior of CE-DYNAM under different scenarios, two simulations were made after model calibration. In Simulation #1 (S1), all ETD-related processes are considered. In Simulation #2 (S2), no ETD-related processes are added to the original LSM fluxes. In this case, the original model is only affected by the vertical discretization of fluxes and the division of soil carbon pools into hillslopes and valley bottoms soil carbon pools. With such assumptions, the summation of

all the results for soil layers of S2 recovers the original LSM results. In both cases, simulations were run from 01/01/1860 to 31/12/2018.

3 Results and discussion

3.1 LSM emulator and erosion rates

The main result for the LSM emulator is presented in Figure 4: a comparison of the true values of ORCHIDEE against the predicted ones from the emulator with ETD not enabled. The simulation was made in one random grid cell representative of the model behaviors over the entire studied region. A slight mismatch between original and predicted values exists at early timesteps, but as expected, values tend to a nearly identical curve after a few timesteps, indicating the adequacy of the emulator to replace the full LSM for erosion calculations with CE-DYNAM. In general, the adoption of an emulator has advantages and disadvantages for CE-DYNAM compared to its implementation directly on an LSM. On the one hand, one can list its simplicity, agility, and flexibility as an advantage to be easily modified for the inclusion of new dynamics, such as the ETD fluxes in the present research, or for other LSMs. It could be noted at this point that practically all existing soil carbon model implementations can be represented in a linear form, and therefore, the matrix approach could be applicable and CE-DYNAM, coupled (Huang et al., 2018). In fact, Sierra and Müller (2015) and Metzler et al. (2020) demonstrate how the approach could be used even for more complex nonlinear models. On the other hand, the use of a standalone version of the LSM allows the processes to be represented only in a simplified way. In the present work, for example, respiration rates and litter input are always assumed to be identical to that simulated by LSM, whereas the literature suggests that, in fact, these should also be affected by ETD fluxes (Olson et al., 2016). Such a limitation also exists for other important interactions affecting the fate of transported carbon that cannot be properly incorporated into the emulator, such as variation in soil moisture and temperature, as well as in organic matter quality and soil fractions (Lal, 2003).

For the erosion rates, Figure 5 and Figure 6 present the historical spatiotemporal variability reconstructed. On the top subfigure of Figure 5, the absolute erosion rates in 1860 are shown on the left, while the maps for 1910, 1960, and 2010 represent the variation with respect to 1860. It can be seen that the annual variations do not follow a linear pattern through time, thus affecting erosion calculations unequally. A decrease in erosion rates from 1860 to 2010 can be noted in Central Europe, and a strong pattern on countries' borders follows from the assumptions of the reconstructed land cover database used (LSCE, 2021). Although partially, this result is related to those reported by Bork and Lang (2003) and Dotterweich (2008), who in historical reconstructions in Germany and Central Europe found peaks in erosion rates in the second half of the 18th century, a period for which there is documentary evidence of extreme rainfall events, and in the early 19th century. In Figure 5, the 1860 erosion map also shows points in four different locations (i.e., P1, P2, P3, and P4, plus the whole study area (WSA)). Within a year, the monthly variations in erosion rates are due solely to changes in the rainfall and the erosivity factor, and as seen on the bottom graph of Figure 5, the pattern of such changes also vary non-linearly in space and may differ from the average pattern of the study area. Additionally, Figure 6 shows the annual average erosion rates, calculated as 2.96 t/ha for 2018. Such a value is higher than the 2.46 t/ha reported by Panagos et al. (2015e), which can be justified by the different spatial

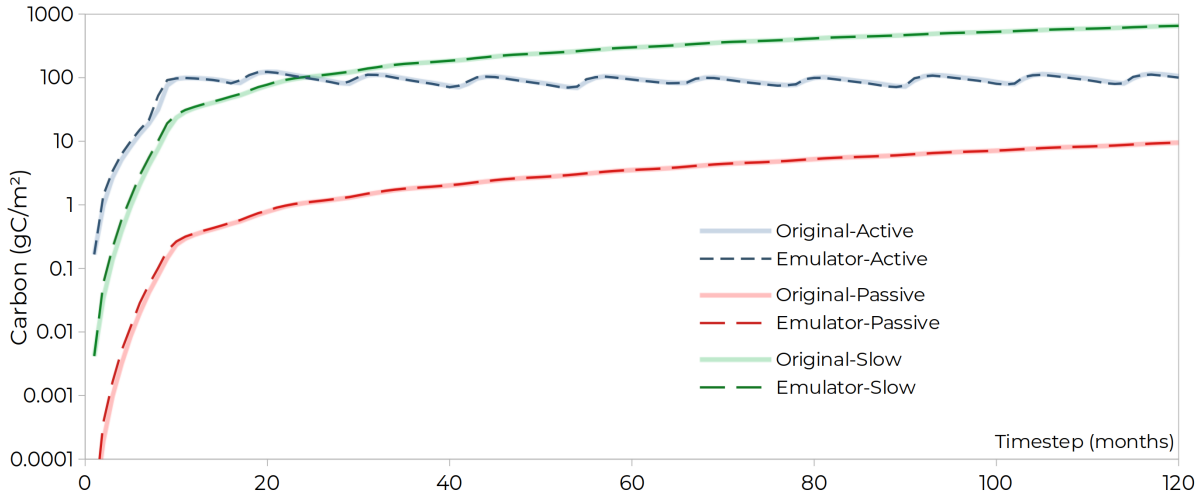

Figure 4. Comparison between the results of the original LSM (i.e., ORCHIDEE, continuous lines) and the results of the emulator constructed for the present work (dashed lines), for 10 years of pools initialization. ORCHIDEE does not have a hillslope-valley bottoms differentiation of pools, while the line for the emulator corresponds to their sum. Ideally, the emulator would be a perfect standalone version of the LSM.

resolution, land cover database, and study area since, in our case, we include Switzerland and the Balkan states, which have erosion rates that are relatively higher compared to their neighbors (Figure 5, top left). Figure 6 also shows the average effect of the two time-varying factors adopted for RUSLE calculation, i.e., the R- and the C-factors of Equation 16. Two distinct patterns of variation can be seen through time, with the R-factor having a higher annual variability and the C-factor being less abrupt except for the evident breaks during the two World Wars. The R-factor shows a cyclic pattern from 1860 to 1901 due to the recycling of (i.e., repetition of climate) forcings adopted by ORCHIDEE for this period. The calculations also indicate an overall increase in erosion rates from 1860-to 1960 due mainly to land cover changes and a peak in rainfall erosivity, followed by an overall decrease from 1960-to 2018. Despite such a pattern in the nearer past, the literature indicates a tipping point in the present. Future projections from Panagos et al. (2021) indicate that water erosion in Europe is expected to increase between 13 and 22.5% by 2050, and Borrelli et al. (2020) estimate an increase in 2015 water erosion rates of 33 to 66% by 2070 worldwide. Under these scenarios, future values could be even higher than the past values calculated and shown in Figure 6.

Also for the erosion rates, the annual country averages were compared against values reported in the literature. The results of Figure 7 (left) show a positive agreement between all databases considered, as highlighted by the positive slope of the robust linear models fitted to the data. The steepness of curves suggests that the model's ability to reproduce the continent-scale patterns is higher than local-scale predictions, which can be interpreted as a consequence of the model's relatively coarse resolution to represent local-scale hydrology. On the right part of Figure 7, the comparison per land cover class shows a close match for croplands and bare soil, the highest rates in our model. On the other hand, our model tends to underestimate erosion

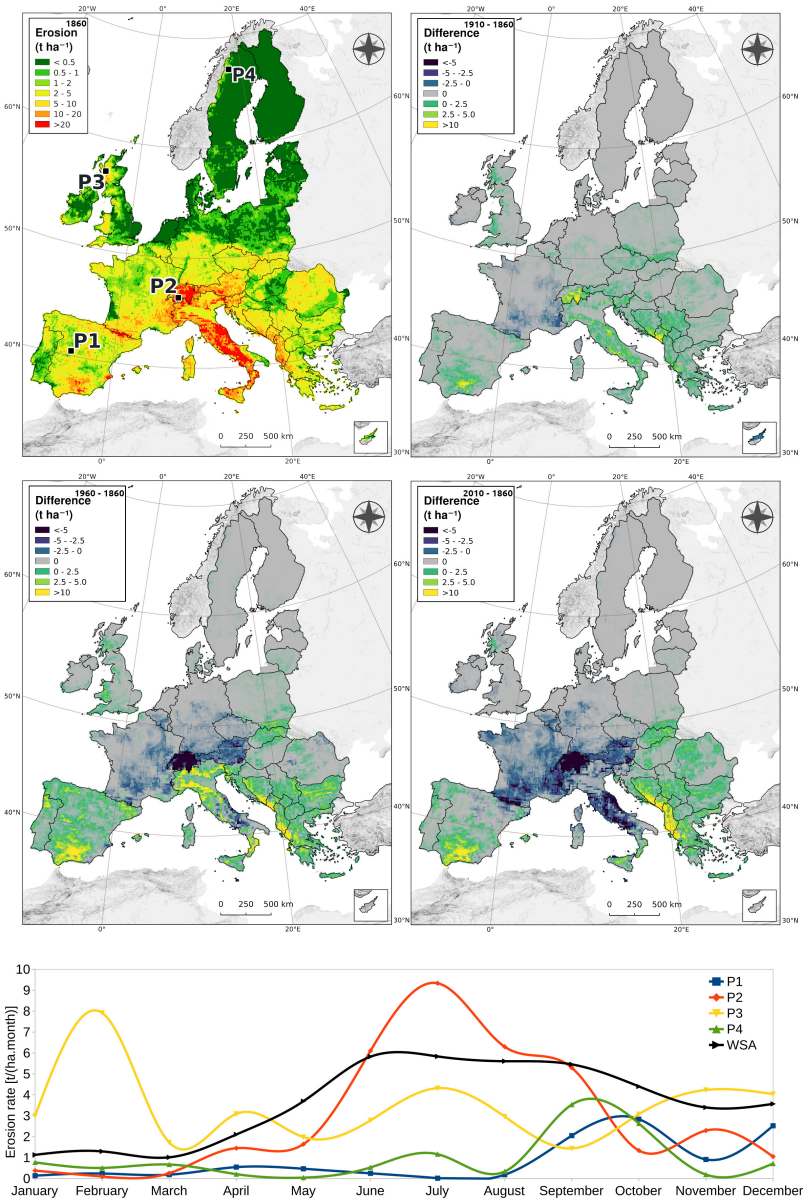

Figure 5. Erosion rates calculated in this work. On the top subfigure, the top-left map shows the erosion rates for 1860 and four points (P1, P2, P3, and P4), while the top-right, bottom-left, and bottom-right maps show the anomalies for 1910, 1960, and 2010, respectively. The bottom subfigure shows the changes in erosion rates due to variations in the monthly rainfall and erosivity for P1, P2, P3, P4, and the whole study area (WSA) within the same year, 1860.

in forests and grasslands compared to the external sources, with our values lying on the lower tail of the distribution of Panagos et al. (2015e) and Cerdan et al. (2010).

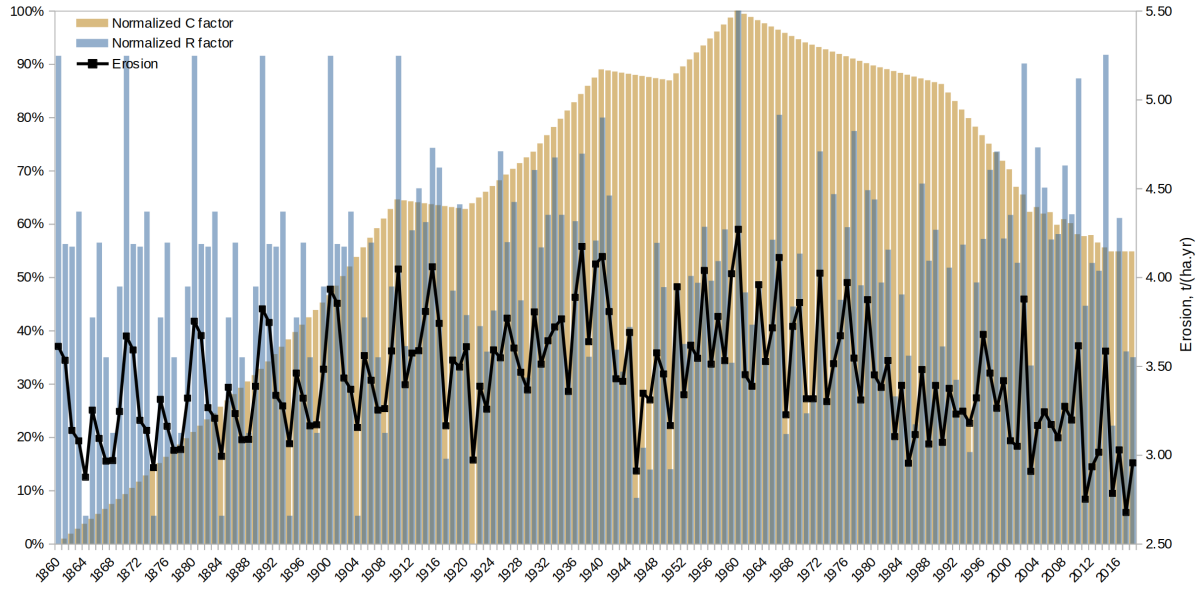

Figure 6. The average impact of the reconstructed R and C-factors on the erosion rates for the period 1860-2018.

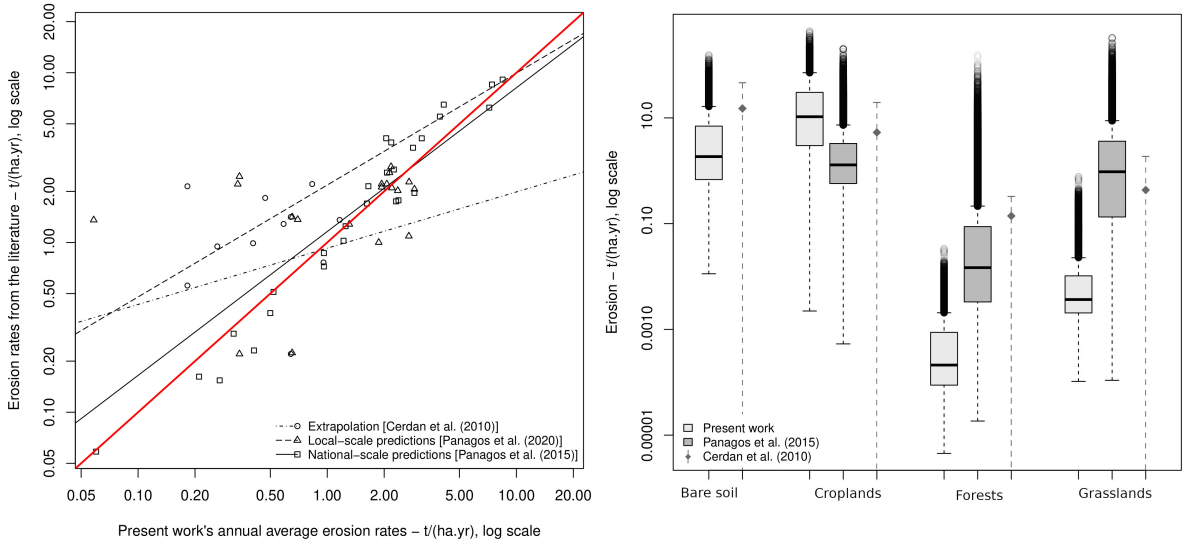

Figure 7. Comparison between the average erosion rates calculated by external sources versus the values calculated in our work, along with an identity line (left); and the comparison of the distribution of erosion rates per land cover (right). In the right plot, the values for our work are the average for the period 1970-2018, and the values for Cerdan et al. (2010) are the reported mean ± standard deviation.

3.2 Model calibration

The NEWUOA algorithm performed several hundred function evaluations until stop. Using averaged annual instead of monthly forcings and performing the calculation only for the catchments areas of stations, each evaluation took around 6 minutes of processing time. The vertical discretization parameter obtained was $\rho_1 = 0.1$, approximately the left pattern from Figure 2. Calibration also indicated that the input of sediments from hillslopes into valley bottoms varies from 0.4 to 11.8% in croplands, from 4.9 to 10.9% in forests, and from 0.3 to 3.8% in grasslands (Figure 8, left). These values can be interpreted in several ways. First, the absolute magnitude of the values is relatively small, following what was suggested by Hoffmann et al. (2013a), with the maximum values being comparable to the 15% of on-site erosion reaching riverine systems presented by Borrelli et al. (2018) for the same study area. However, the direct comparison of these values should be read with caution because of the large methodological differences between works. For example, the authors defined the rivers explicitly and used a higher spatial resolution for a single moment in time, characteristics that contrast with those of CE-DYNAM (Naipal et al., 2020). Furthermore, despite the similar interpretation, the quantities compared may themselves differ between the models adopted (Rompaey et al., 2001). Second, regarding the shape of the curves, there is an increasing relation in parameter g_f as a function of slope for forests and croplands but a decreasing relation for grasslands. The increase in two of the three land-use classes can be readily explained by the important effect of gravity on sediment transport (Bridge, 2003; Huggett, 2017), while its generally low range of values can partially explain the unexpected decrease in grasslands compared to that of forests and croplands. Third, with respect to the ordering of the curves, two patterns are observed. In flat areas, with a slope less than 1.5°, the pattern is forests having higher transport than grasslands, followed by croplands. In steeper areas, with slopes above 1.5°, there is a rapid change in the ordering, leading to a situation where croplands generally have higher sediment transport than forests and grasslands. The low influence of this region on sediment production can explain the non-intuitive relationship between the classes. For example, areas with slopes less than 1.5° were responsible for only 5.43% of Europe's total erosion in 2018, with the remaining 94.57% occurring in the steeper areas. Therefore, it is reasonable to expect that the steeper areas will be better represented in the model. Thus, the latter pattern of Figure 8 can be explained by the lower cohesive properties of the less vegetated covers relative to the more vegetated ones, consequently offering less resistance to water and sediment flow (Osterkamp et al., 2011; Hoffmann et al., 2013a; Huggett, 2017). Figure 8, right, also shows the sediment residence time, which was estimated to vary from 0.5 years (180 days) to 24.5 years, indicating that sediment retention increases with watershed size, in agreement with that described by Hoffmann et al. (2013b).

The validation for the best set of parameters is summarized in Figure 9, which shows a plot of actual against predicted values (using annual forcings) for the observed and the unobserved locations. In all cases, the prediction value used for this comparison are those from the same year as the observation. The red diagonal is a 1:1 line, and each group of dots connected by a line represents a different station. The best set of parameters found yielded ME $= 0.603$ and $R^2 = 0.666$ for the observed stations, and ME $= 0.152$ and $R^2 = 0.438$ for the unobserved stations. Overall, for the full dataset, the model has a ME $= 0.578$ and $R^2 = 0.640$. The values obtained are relatively high when compared to similar studies. Works such as that of Feng et al. (2010) and Rompaey et al. (2005) in China and Italy, respectively, reported negative ME values, which indicate

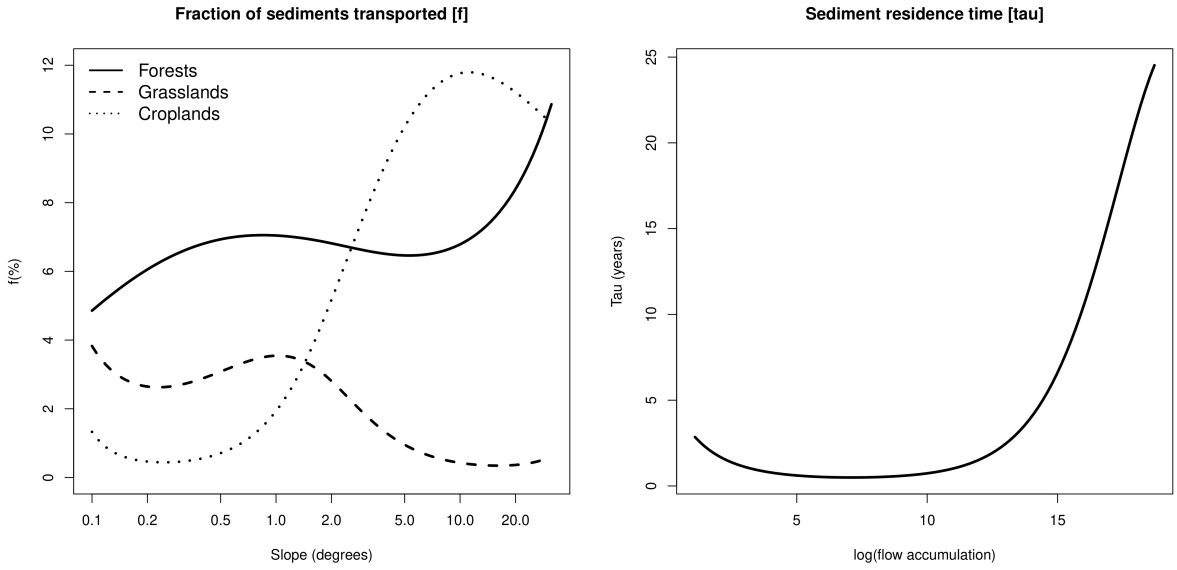

Figure 8. Results from the calibration procedure: the fraction of sediments that go from hillslopes to valley bottoms (left), and sediment residence time (right).

that sometimes distributed models are unable to represent sediment dynamics, especially when there is high heterogeneity in the data (Rompaey et al., 2005). In Quijano et al. (2016), where the authors studied four adjacent hydrological units at a local scale in Spain, distributed models well could represented well the dynamics involved. The overall value obtained for the study region was ME $= 0.11$, while the value calculated individually per hydrological unit ranged from ME $= -0.11$ to ME $= 0.49$. In what is probably the most similar to our work in terms of the study area, Borrelli et al. (2018) initially considered a total of 24 semi-natural and agricultural basins in Europe, for which they obtained ME = 0.38. The result motivated the authors to further remove basins as a fine-tuning of the model calibration used, which led to a ME $= 0.89$ for ten basins. The results from these other studies help us to compare the performance of the model presented in the current work. It can be noted that the present work uses more observations and calibrates the model with time-varying data (i.e., not long-term averages), which requires a more complex model architecture and highlight the robustness of the calibration performed. It is also an important remark that the comparison with other works was only possible after the methodological improvements in the new version of CE-DYNAM compared to that of Naipal et al. (2020): i) the possibility of calibrating the lateral fluxes using sediment data collected in the field and relatively abundant in the literature (see United Nations Environment Programme, 2018); ii) the possibility of performing validation with field data, using the model as a basis for prediction for locations unobserved during its fit.

We also used the same best set of parameters with monthly forcings to quantify how distant the simplified calibration with annual forcings is from the optimal condition. Using monthly forcings for a full calibration remains precluded since a single

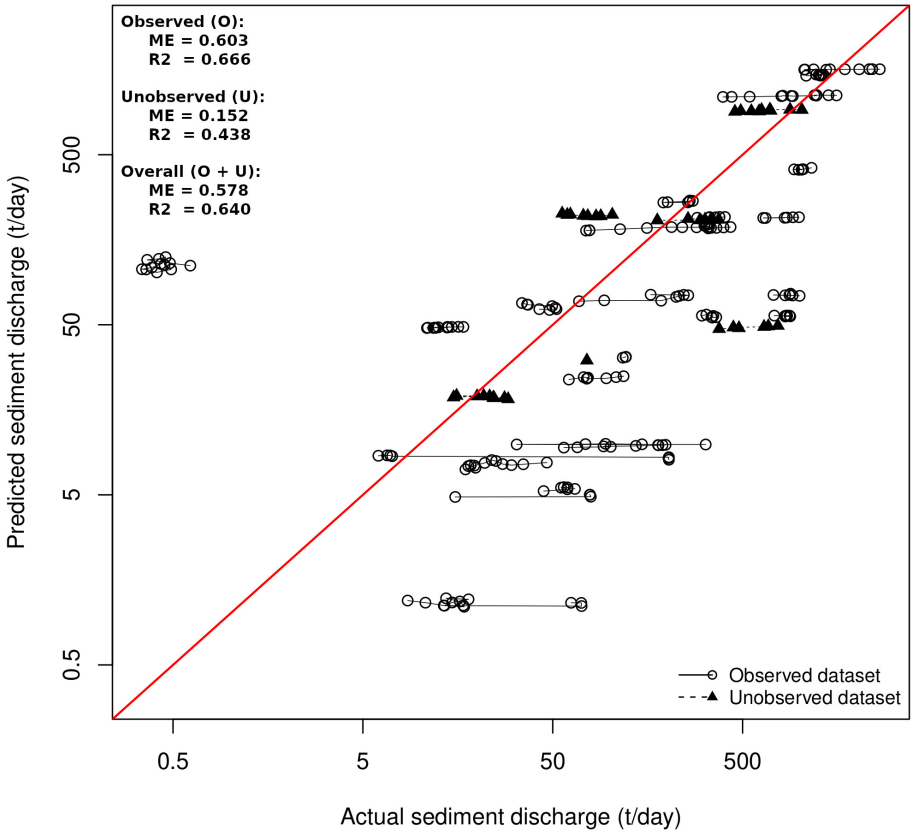

Figure 9. Plot of the predicted annual averages against the observed annual sediment discharged values in log scale. Each dot or triangle corresponds to one of the 241 observations, and the connected icons correspond to one of the 30 different stations of the database. The red line is an identity line.

function evaluation took almost one day to complete. In that experiment, values dropped to ME $= 0.464$ and $R^2 = 0.616$ for the entire dataset, indicating a relatively small change in predictions compared to the simplification using annual forcings.

3.3 Simulations

In both scenarios, the two A matrices (i.e., one for hillslopes and the other for valley bottoms calculation) are square with a size equal to the product between the number of cells, the number of PFTs, the number of soil layers and the number of soil carbon pools, which for the setting used in the present work equals $1.85 \cdot 10^7$ rows and columns. In S1, where all fluxes are considered, the average number of non-zero elements on the A matrices of hillslopes and valley bottoms were $7.4 \cdot 10^6$ and $1.7 \cdot 10^7$, respectively, corresponding to densities of 21.6 ppb (i.e., 10^{-9}) and 49.7 ppb. In S2, where fewer fluxes are simulated, the A matrices for hillslopes and valley bottoms contained $5.9 \cdot 10^6$ and $7.4 \cdot 10^6$, yielding a density of 17.2 ppb and 21.6 ppb,

respectively. Simulations were run on a High-Performance Computer having 19 Intel(R) Xeon(R) CPU E5-2640 v4 2.40 GHz processors. The number of cores used for calculations varied, as specified next. In both scenarios, the generation of A and B took around 3 to 6 minutes for each simulation month at the continent scale. After the generation of all matrices, equilibrium calculation took around 10 minutes on a single core. As a comparison, the calculation for the non-alpine region of the Rhine basin of Naipal et al. (2020) used to take two days in seven cores of the same machine. The drastic reduction is a consequence of the matrix approach adopted. While in their work all fluxes had to be recalculated for each month of equilibrium calculation, in our case we just had to precalculate A and B once.

The matrix approach brought several benefits for speeding up the model. First, the analytical representation of the model allowed the derivation of first-order approximations for the monthly averages, which are faster to calculate than summing the daily simulations and dividing by the number of days. Second, despite the different settings of S1 and S2, implementation was straightforward thanks to the natural interpretation of each element of A as a flux of carbon from one to another uniquely identified combination carbon pool. Third, the calculation of A and B are independent for each month, which drastically increases the number of possible concurrent execution threads in comparison to the original model of Naipal et al. (2020). These results are similar to those found in the literature. For example, Xia et al. (2012) and Huang et al. (2018) reported reduced processing time and computational cost of the calculations. In our case, it is not possible to compare the processing times as done by Xia et al. (2012) because the previous version of the CE-DYNAM from Naipal et al. (2020) does not support the calculation at a continental scale in a feasible time. In this sense, the very possibility of applying the model at this scale, now allowed because of the matrix approach, is an indicator of such improvements. However, the matrix approach may require changes for applications at even larger scales, such as the global scale. As shown in Equation 2, the approach simplifies the simulation by representing the variation of fluxes with additions and matrix-vector multiplications. Such operations are typically efficient in the format known as Compressed Sparse Row (CSR) (Bai, 2000; Greathouse and Daga, 2014), which requires the storage of three vectors for its construction. In global scale problems, it is possible that the amount of memory required for such storage is excessively large, so alternative representations should be explored. A possible solution may come from an analogous problem in the statistical regression literature, where authors seek low-rank representations of models in order to reduce the dimensionality of the problem while still largely preserving the characteristics of the original model (see Wang and Ranalli (2006) and Wood (2006) for two examples). However, while procedures that are central for dimensionality reduction problems such as singular value decomposition are well established for dense matrices (Strang, 2016) or even sparse matrices of reasonable size, the problem can be complicated when the dimensions are huge. Therefore, further research and work to search for applicable methods are needed.

The calculation for a depositional site indicates that the additional incoming fluxes from its upstream area due to ETD processes tend to increase the carbon stock at the site from 6,800 to 7,150 g/m^2 at equilibrium, equivalent to a 5.1% increase (Figure 10, top). Figure 10, bottom, illustrates the ability of the model to emulate non-linearities on the impact of ETD fluxes on the carbon cycle. The results are supposed to represent the impacts of the ETD fluxes on the carbon cycle of a depositional area. According to van Oost et al. (2005), Li et al. (2007), and Wang et al. (2015), some of the expected changes in the dynamics include an increase in the C burial, resulting in an increase of the soil organic carbon, as well as enhanced respiration of the

carbon buried with time (Naipal et al., 2020). In fact, in the early period of the curve, from 1860 to approximately 1940, the curve of the S1 simulation is above that of the S2 simulation, indicating that the immediate impact of adding new fluxes to an area is to increase the rates of carbon burial. However, in the final period of the curve, from 1941 to 2018, the variation curve of S1 moves below the S2 curve, indicating a decrease in the lateral input and the rate of carbon burial, as well as a higher respiration by microorganisms due to the carbon previously buried.

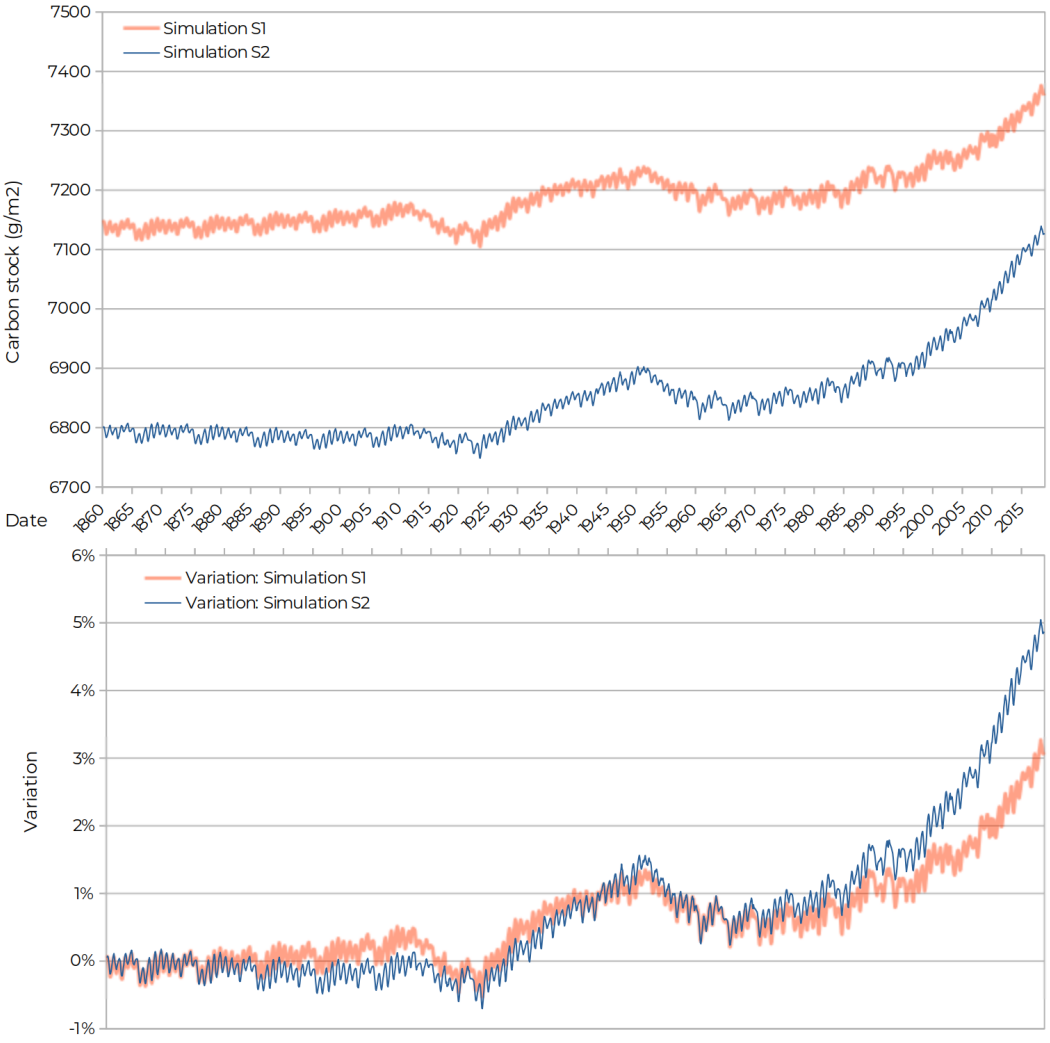

Figure 10. Results for the depositional site: absolute values of carbon stock (g/m^2) (top), relative difference (bottom).

Furthermore, to check the mass balance closure, all the fluxes from this depositional area were calculated from 1860 to 2018. On the cell's hillslope fraction, litter input added 25,404.47 gC/m^2 and land cover added 128.71 gC/m^2, of which 25,286.00 gC/m^2 were respired, and 0.39 gC/m^2 were sent to the valley bottoms. On the valley bottom fraction, the inputs were: 0.39

gC/m^2 coming from the hillslopes, 722.16 gC/m^2 from upstream lands, and 6,039.23 gC/m^2 from litter. Of this, 6,764.07 gC/m^2 was respired, and 23.91 gC/m^2 was lost due to land cover change. These values indicate that local erosion at this depositional area is not relevant to the carbon cycle, in contrast to the carbon input from upstream lands, which corresponded to 10.68% of all the valley bottom fraction inputs.

4 Limitations

Despite the advances presented in this work, there are still limitations that need to be addressed with future modifications. Concerning its structure, incorporating sediment data in CE-DYNAM is only possible by assuming that sediment and carbon follow the same dynamics. While this is convenient for calibration, it might not be realistic, so further work is necessary to improve this important assumption. Besides, the physical representation of the fluxes could be improved. For example, no transformation of C pools during the transport process is represented, such as the breakdown of aggregates. In practice, they could increase the turnover rates of soil organic carbon compared to the simulations we presented.

Regarding the calibration presented here, other limitations concern the spatial resolution and historical reconstructions. First, finding the optimal resolution for CE-DYNAM will always be a problem since it is halfway between the fine-scale hydrological processes it represents and the coarse resolution of the current climate models. Second, the historical reconstructions presented are highly sensitive to the assumptions adopted and presented. Even though these assumptions are properly evaluated during the calibration and validation process, better results will be possible the better the input maps for the model are.

Another important limitation refers to the structure of the calibration parameters. The structure presented in this work allows a certain balance between the share of sediments that move from hillslopes to valley bottoms and the sediment residence time, so that the optimization may sometimes tend to yield physically unrealistic results. In the present work, this was solved by using multiple starting points, but a better solution in the future should come from the development of the model itself to penalize solutions that do not have a meaningful physical interpretation. Finally, our model also naturally inherits the problems of some necessary assumptions. Even the fundamental assumption that calculations converge to the pullback attracting trajectory in 1860-1869 might not be correct and affect the results largely (Sanderman et al., 2017; Dimassi et al., 2018). Analogously, the RUSLE-based approach for erosion modeling is widely criticized, but remains the sole alternative for large-scale quantitative applications (Panagos et al., 2016).

5 Conclusions

In this paper, we addressed the challenge of scaling CE-DYNAM, an erosion-transport-deposition model, in a relatively high spatial resolution and long period at the European scale. First, we show how the lateral fluxes of CE-DYNAM can be represented in a matrix form, an alternative that allows the acceleration of the computations performed, making them feasible for large-scale applications. Our work, therefore, enabled the previously precluded possibility of applying CE-DYNAM to large spatial domains or high spatial resolutions. We also improved the model's physical representation of sediment movement to

allow for proper calibration and validation procedures using observations of sediment discharge collected on the field. With these changes, the presented model can be readily adapted to other study regions, the main limiting factor being the availability of inputs from external sources. We also describe how the proposed technical solution might not work on an even larger scale (global scale, for example), so further work may be needed to improve the proposed approach, such as the search for computation of low-rank representations of the model matrices.

Second, a more practical contribution of our work was the calibration of the model for the whole of Europe from field-collected data. Our results show that the patterns obtained are internally consistent and coherent with those previously reported in the literature in similar work. We expect the patterns obtained in this work to serve as a reference for future models for this study region. Since the calibration of the lateral fluxes is done using sediment data, the results form the basis for simulations of the impact of erosion on the carbon cycle and the future incorporation of other nutrients, such as nitrogen and phosphorus, into CE-DYNAM. These works could advance our understanding of the role of ETD processes on nutrient cycles.

Third, we used the calibrated model to predict the movement of carbon at a depositional site, the type of site that tends to be highly affected by incoming lateral fluxes from upstream lands. This simulation evaluated the model's impact on soil carbon pools and showed how the effect of erosion on the carbon cycle could be nonlinear in time. In this sense, this result shows that time-static models can only partially disclose the correct effect of ETD on the carbon cycle.

Code availability. The codes are available at: https://doi.org/10.5281/zenodo.6553890. The dataset used can be made available under request to the corresponding author. Access to the data used in the paper has been granted to the Editor and Reviewers during the peer-review process.

Author contributions.

- *Arthur Nicolaus Fendrich*: Conceptualization, Investigation, Methodology, Data curation, Validation, Formal analysis, Writing - original draft, Writing – review & editing.
- *Philippe Ciais*: Conceptualization, Investigation, Methodology, Writing - original draft, Funding acquisition, Supervision.
- *Emanuele Lugato*: Conceptualization, Investigation, Methodology, Validation, Writing – original draft.
- *Marco Carozzi*: Conceptualization, Investigation, Methodology, Validation, Writing – original draft.
- *Bertrand Guenet*: Conceptualization, Investigation, Methodology, Writing – original draft.
- *Victoria Naipal*: Conceptualization, Methodology, Writing – original draft.
- *Matthew McGrath*: Investigation, Data curation, Methodology, Writing – original draft.
- *Philippe Martin*: Conceptualization, Investigation, Methodology, Writing - original draft, Funding acquisition, Supervision.
- *Panos Panagos*: Conceptualization, Investigation, Methodology, Writing - original draft, Funding acquisition, Supervision.

Competing interests. The authors declare that the research was conducted in the absence of any commercial or financial relationships that could be construed as a potential conflict of interest.

Acknowledgements. This work was realised with the collaboration of the European Commission Joint Research Centre under the Collaborative Doctoral Partnership Agreement No. 35403, and partially funded by the CLAND project. The authors would like to thank Philippe Peylin for granting access to the high-resolution VERIFY forcings, Francis Matthews for the constructive discussions about model calibration, Leonidas Liakos for the European map layouts, Gerd Sparovek for the comments prior to the submission, and Lucas Resende for reviewing the mathematical notation.

References

Bai, Z.: Templates for the solution of algebraic eigenvalue problems : a practical guide, Society for Industrial and Applied Mathematics (SIAM, 3600 Market Street, Floor 6, Philadelphia, PA 19104, Philadelphia, Pa, 2000.

Ballabio, C., Borrelli, P., Spinoni, J., Meusburger, K., Michaelides, S., Beguería, S., Klik, A., Petan, S., Janeček, M., Olsen, P., Aalto, J., Lakatos, M., Rymszewicz, A., Dumitrescu, A., Tadić, M. P., Diodato, N., Kostalova, J., Rousseva, S., Banasik, K., Alewell, C., and Panagos, P.: Mapping monthly rainfall erosivity in Europe, Science of The Total Environment, 579, 1298–1315, https://doi.org/10.1016/j.scitotenv.2016.11.123, 2017.

Bonan, G. B. and Doney, S. C.: Climate, ecosystems, and planetary futures: The challenge to predict life in Earth system models, Science, 359, eaam8328, https://doi.org/10.1126/science.aam8328, 2018.

Bork, H.-R. and Lang, A.: Quantification of past soil erosion and land use / land cover changes in Germany, in: Long Term Hillslope and Fluvial System Modelling, pp. 231–239, Springer Berlin Heidelberg, https://doi.org/10.1007/3-540-36606-7_12, 2003.

Borrelli, P., van Oost, K., Meusburger, K., Alewell, C., Lugato, E., and Panagos, P.: A step towards a holistic assessment of soil degradation in Europe: Coupling on-site erosion with sediment transfer and carbon fluxes, Environmental Research, 161, 291–298, https://doi.org/10.1016/j.envres.2017.11.009, 2018.

Borrelli, P., Robinson, D. A., Panagos, P., Lugato, E., Yang, J. E., Alewell, C., Wuepper, D., Montanarella, L., and Ballabio, C.: Land use and climate change impacts on global soil erosion by water (2015-2070), Proceedings of the National Academy of Sciences, 117, 21 994–22 001, https://doi.org/10.1073/pnas.2001403117, 2020.

Bridge, J. S.: Rivers and floodplains : forms, processes, and sedimentary record, Blackwell Pub, Oxford, UK Malden, MA, USA, 2003.

Camino-Serrano, M., Guenet, B., Luyssaert, S., Ciais, P., Bastrikov, V., Vos, B. D., Gielen, B., Gleixner, G., Jornet-Puig, A., Kaiser, K., Kothawala, D., Lauerwald, R., Peñuelas, J., Schrumpf, M., Vicca, S., Vuichard, N., Walmsley, D., and Janssens, I. A.: ORCHIDEE-SOM: modeling soil organic carbon (SOC) and dissolved organic carbon (DOC) dynamics along vertical soil profiles in Europe, Geoscientific Model Development, 11, 937–957, https://doi.org/10.5194/gmd-11-937-2018, 2018.

Cerdan, O., Govers, G., Bissonnais, Y. L., van Oost, K., Poesen, J., Saby, N., Gobin, A., Vacca, A., Quinton, J., Auerswald, K., Klik, A., Kwaad, F., Raclot, D., Ionita, I., Rejman, J., Rousseva, S., Muxart, T., Roxo, M., and Dostal, T.: Rates and spatial variations of soil erosion in Europe: A study based on erosion plot data, Geomorphology, 122, 167–177, https://doi.org/10.1016/j.geomorph.2010.06.011, 2010.

Chang, J., Ciais, P., Gasser, T., Smith, P., Herrero, M., Havlík, P., Obersteiner, M., Guenet, B., Goll, D. S., Li, W., Naipal, V., Peng, S., Qiu, C., Tian, H., Viovy, N., Yue, C., and Zhu, D.: Climate warming from managed grasslands cancels the cooling effect of carbon sinks in sparsely grazed and natural grasslands, Nature Communications, 12, https://doi.org/10.1038/s41467-020-20406-7, 2021.

Ciais, P., Sabine, C., Bala, G., Bopp, L., Brovkin, V., et al.: Carbon and other biogeochemical cycles, in: Climate Change 2013 - The Physical Science Basis, pp. 465–570, Cambridge University Press, 2013.

Corless, R. M., Gonnet, G. H., Hare, D. E. G., Jeffrey, D. J., and Knuth, D. E.: On the Lambert W function, Advances in Computational Mathematics, 5, 329–359, https://doi.org/10.1007/bf02124750, 1996.

de Roo, A., Jetten, V., Wesseling, C., and Ritsema, C.: LISEM: A Physically-Based Hydrologic and Soil Erosion Catchment Model, in: Modelling Soil Erosion by Water, pp. 429–440, Springer Berlin Heidelberg, https://doi.org/10.1007/978-3-642-58913-3_32, 1998.

Dimassi, B., Guenet, B., Saby, N. P., Munoz, F., Bardy, M., Millet, F., and Martin, M. P.: The impacts of CENTURY model initialization scenarios on soil organic carbon dynamics simulation in French long-term experiments, Geoderma, 311, 25–36, https://doi.org/10.1016/j.geoderma.2017.09.038, 2018.

Dotterweich, M.: The history of soil erosion and fluvial deposits in small catchments of central Europe: Deciphering the long-term interaction between humans and the environment — A review, Geomorphology, 101, 192–208, https://doi.org/10.1016/j.geomorph.2008.05.023, 2008.

European Commission: European Green Deal, https://ec.europa.eu/clima/eu-action/european-green-deal_en, 2021.

European Spatial Agency: Climate Change Initiative, https://www.esa-landcover-cci.org/, 2021.

European Union: The EU - what it is and what it does, https://doi.org/10.2775/946008, 2021.

Everitt, B. S. and Skrondal, A.: The Cambridge Dictionary of Statistics, Cambridge University Press, hardcover edn., 2010.

Farr, T. G., Rosen, P. A., Caro, E., Crippen, R., Duren, R., et al.: The Shuttle Radar Topography Mission, Reviews of Geophysics, 45, https://doi.org/https://doi.org/10.1029/2005RG000183, 2007.

Feng, X., Wang, Y., Chen, L., Fu, B., and Bai, G.: Modeling soil erosion and its response to land-use change in hilly catchments of the Chinese Loess Plateau, Geomorphology, 118, 239–248, https://doi.org/10.1016/j.geomorph.2010.01.004, 2010.

Friedlingstein, P.: Carbon cycle feedbacks and future climate change, Philosophical Transactions of the Royal Society A: Mathematical, Physical and Engineering Sciences, 373, 20140 421, https://doi.org/10.1098/rsta.2014.0421, 2015.

Friedlingstein, P., Cox, P., Betts, R., Bopp, L., von Bloh, W., Brovkin, V., Cadule, P., Doney, S., Eby, M., Fung, I., Bala, G., John, J., Jones, C., Joos, F., Kato, T., Kawamiya, M., Knorr, W., Lindsay, K., Matthews, H. D., Raddatz, T., Rayner, P., Reick, C., Roeckner, E., Schnitzler, K.-G., Schnur, R., Strassmann, K., Weaver, A. J., Yoshikawa, C., and Zeng, N.: Climate–Carbon Cycle Feedback Analysis: Results from the C4MIP Model Intercomparison, Journal of Climate, 19, 3337–3353, https://doi.org/10.1175/jcli3800.1, 2006.

Gatti, L. V., Basso, L. S., Miller, J. B., Gloor, M., Domingues, L. G., et al.: Amazonia as a carbon source linked to deforestation and climate change, Nature, 595, 388–393, https://doi.org/10.1038/s41586-021-03629-6, 2021.

Gettelman, A. and Rood, R. B.: Demystifying Climate Models, Springer Berlin Heidelberg, https://doi.org/10.1007/978-3-662-48959-8, 2016.

Greathouse, J. L. and Daga, M.: Efficient Sparse Matrix-Vector Multiplication on GPUs Using the CSR Storage Format, in: SC14: International Conference for High Performance Computing, Networking, Storage and Analysis, IEEE, https://doi.org/10.1109/sc.2014.68, 2014.

Guenet, B., Gabrielle, B., Chenu, C., Arrouays, D., Balesdent, J., Bernoux, M., Bruni, E., Caliman, J.-P., Cardinael, R., Chen, S., Ciais, P., Desbois, D., Fouche, J., Frank, S., Henault, C., Lugato, E., Naipal, V., Nesme, T., Obersteiner, M., Pellerin, S., Powlson, D. S., Rasse, D. P., Rees, F., Soussana, J.-F., Su, Y., Tian, H., Valin, H., and Zhou, F.: Can N2O emissions offset the benefits from soil organic carbon storage?, Global Change Biology, 27, 237–256, https://doi.org/10.1111/gcb.15342, 2020.

Hamaoui-Laguel, L., Vautard, R., Liu, L., Solmon, F., Viovy, N., Khvorostyanov, D., Essl, F., Chuine, I., Colette, A., Semenov, M. A., Schaffhauser, A., Storkey, J., Thibaudon, M., and Epstein, M. M.: Effects of climate change and seed dispersal on airborne ragweed pollen loads in Europe, Nature Climate Change, 5, 766–771, https://doi.org/10.1038/nclimate2652, 2015.

Harper, A. B., Powell, T., Cox, P. M., House, J., Huntingford, C., Lenton, T. M., Sitch, S., Burke, E., Chadburn, S. E., Collins, W. J., Comyn-Platt, E., Daioglou, V., Doelman, J. C., Hayman, G., Robertson, E., van Vuuren, D., Wiltshire, A., Webber, C. P., Bastos, A., Boysen, L., Ciais, P., Devaraju, N., Jain, A. K., Krause, A., Poulter, B., and Shu, S.: Land-use emissions play a critical role in land-based mitigation for Paris climate targets, Nature Communications, 9, https://doi.org/10.1038/s41467-018-05340-z, 2018.

Hoffmann, T., Mudd, S. M., van Oost, K., Verstraeten, G., Erkens, G., Lang, A., Middelkoop, H., Boyle, J., Kaplan, J. O., Willenbring, J., and Aalto, R.: Short Communication: Humans and the missing C-sink: erosion and burial of soil carbon through time, Earth Surface Dynamics, 1, 45–52, https://doi.org/10.5194/esurf-1-45-2013, 2013a.

Hoffmann, T., Schlummer, M., Notebaert, B., Verstraeten, G., and Korup, O.: Carbon burial in soil sediments from Holocene agricultural erosion, Central Europe, Global Biogeochemical Cycles, 27, 828–835, https://doi.org/10.1002/gbc.20071, 2013b.

Huang, Y., Lu, X., Shi, Z., Lawrence, D., Koven, C. D., Xia, J., Du, Z., Kluzek, E., and Luo, Y.: Matrix approach to land carbon cycle modeling: A case study with the Community Land Model, Global Change Biology, 24, 1394–1404, https://doi.org/10.1111/gcb.13948, 2017.

Huang, Y., Zhu, D., Ciais, P., Guenet, B., Huang, Y., Goll, D. S., Guimberteau, M., Jornet-Puig, A., Lu, X., and Luo, Y.: Matrix-Based Sensitivity Assessment of Soil Organic Carbon Storage: A Case Study from the ORCHIDEE-MICT Model, Journal of Advances in Modeling Earth Systems, 10, 1790–1808, https://doi.org/https://doi.org/10.1029/2017MS001237, 2018.

Huggett, R.: Fundamentals of geomorphology, Routledge, London New York, NY, 2017.

IPCC: Climate change and land : an IPCC special report on climate change, desertification, land degradation, sustainable land management, food security, and greenhouse gas fluxes in terrestrial ecosystems : summary for policymakers, Intergovernmental Panel on Climate Change, Geneva, 2019.

Kinnell, P.: Event soil loss, runoff and the Universal Soil Loss Equation family of models: A review, Journal of Hydrology, 385, 384–397, https://doi.org/10.1016/j.jhydrol.2010.01.024, 2010.

Krinner, G., Viovy, N., de Noblet-Ducoudré, N., Ogée, J., Polcher, J., Friedlingstein, P., Ciais, P., Sitch, S., and Prentice, I. C.: A dynamic global vegetation model for studies of the coupled atmosphere-biosphere system, Global Biogeochemical Cycles, 19, https://doi.org/10.1029/2003gb002199, 2005.

Lal, R.: Soil erosion and the global carbon budget, Environment International, 29, 437–450, https://doi.org/10.1016/s0160-4120(02)00192-7, 2003.

Lal, R.: Accelerated Soil erosion as a source of atmospheric CO2, Soil and Tillage Research, 188, 35–40, https://doi.org/10.1016/j.still.2018.02.001, 2019.

Lehner, B., Verdin, K., and Jarvis, A.: New Global Hydrography Derived From Spaceborne Elevation Data, Eos, Transactions American Geophysical Union, 89, 93–94, https://doi.org/https://doi.org/10.1029/2008EO100001, 2008.

Leng, G. and Hall, J.: Crop yield sensitivity of global major agricultural countries to droughts and the projected changes in the future, Science of The Total Environment, 654, 811–821, https://doi.org/https://doi.org/10.1016/j.scitotenv.2018.10.434, 2019.

Li, Y., Zhang, Q. W., Reicosky, D. C., Lindstrom, M. J., Bai, L. Y., and Li, L.: Changes in soil organic carbon induced by tillage and water erosion on a steep cultivated hillslope in the Chinese Loess Plateau from 1898–1954 and 1954–1998, Journal of Geophysical Research, 112, https://doi.org/10.1029/2005jg000107, 2007.

LSCE: ORCHIDEE Development Section. Land Cover - Description, https://orchidas.lsce.ipsl.fr/dev/lccci/, Online; accessed 15 September 2021, 2021.

Lu, X., Du, Z., Huang, Y., Lawrence, D., Kluzek, E., Collier, N., Lombardozzi, D., Sobhani, N., Schuur, E. A. G., and Luo, Y.: Full Implementation of Matrix Approach to Biogeochemistry Module of CLM5, Journal of Advances in Modeling Earth Systems, 12, e2020MS002 105, https://doi.org/https://doi.org/10.1029/2020MS002105, e2020MS002105 2020MS002105, 2020.

Lugato, E., Smith, P., Borrelli, P., Panagos, P., Ballabio, C., et al.: Soil erosion is unlikely to drive a future carbon sink in Europe, Science Advances, 4, eaau3523, https://doi.org/10.1126/sciadv.aau3523, 2018.

Luo, Y., Shi, Z., Lu, X., Xia, J., Liang, J., Jiang, J., Wang, Y., Smith, M. J., Jiang, L., Ahlström, A., Chen, B., Hararuk, O., Hastings, A., Hoffman, F., Medlyn, B., Niu, S., Rasmussen, M., Todd-Brown, K., and Wang, Y.-P.: Transient dynamics of terrestrial carbon storage: mathematical foundation and its applications, Biogeosciences, 14, 145–161, https://doi.org/10.5194/bg-14-145-2017, 2017.

Metzler, H., Zhu, Q., Riley, W., Hoyt, A., Müller, M., and Sierra, C. A.: Mathematical Reconstruction of Land Carbon Models From Their Numerical Output: Computing Soil Radiocarbon From C Dynamics, Journal of Advances in Modeling Earth Systems, 12, https://doi.org/10.1029/2019ms001776, 2020.

Minasny, B., Malone, B. P., McBratney, A. B., Angers, D. A., Arrouays, D., Chambers, A., Chaplot, V., Chen, Z.-S., Cheng, K., Das, B. S., Field, D. J., Gimona, A., Hedley, C. B., Hong, S. Y., Mandal, B., Marchant, B. P., Martin, M., McConkey, B. G., Mulder, V. L., O'Rourke, S., de Forges, A. C. R., Odeh, I., Padarian, J., Paustian, K., Pan, G., Poggio, L., Savin, I., Stolbovoy, V., Stockmann, U., Sulaeman, Y., Tsui, C.-C., Vågen, T.-G., van Wesemael, B., and Winowiecki, L.: Soil carbon 4 per mille, Geoderma, 292, 59–86, https://doi.org/10.1016/j.geoderma.2017.01.002, 2017.

Montanarella, L. and Panagos, P.: The relevance of sustainable soil management within the European Green Deal, Land Use Policy, 100, 104 950, https://doi.org/10.1016/j.landusepol.2020.104950, 2021.

Naipal, V., Reick, C., Pongratz, J., and van Oost, K.: Improving the global applicability of the RUSLE model – adjustment of the topographical and rainfall erosivity factors, Geoscientific Model Development, 8, 2893–2913, https://doi.org/10.5194/gmd-8-2893-2015, 2015.

Naipal, V., Reick, C., van Oost, K., Hoffmann, T., and Pongratz, J.: Modeling long-term, large-scale sediment storage using a simple sediment budget approach, Earth Surface Dynamics, 4, 407–423, https://doi.org/10.5194/esurf-4-407-2016, 2016.

Naipal, V., Lauerwald, R., Ciais, P., Guenet, B., and Wang, Y.: CE-DYNAM (v1): a spatially explicit process-based carbon erosion scheme for use in Earth system models, Geoscientific Model Development, 13, 1201–1222, https://doi.org/10.5194/gmd-13-1201-2020, 2020.

Nash, J. and Sutcliffe, J.: River flow forecasting through conceptual models part I — A discussion of principles, Journal of Hydrology, 10, 282–290, https://doi.org/10.1016/0022-1694(70)90255-6, 1970.

Nobre, C. A., Sampaio, G., Borma, L. S., Castilla-Rubio, J. C., Silva, J. S., et al.: Land-use and climate change risks in the Amazon and the need of a novel sustainable development paradigm, Proceedings of the National Academy of Sciences, 113, 10 759–10 768, https://doi.org/10.1073/pnas.1605516113, 2016.

Olson, K. R., Al-Kaisi, M., Lal, R., and Cihacek, L.: Impact of soil erosion on soil organic carbon stocks, Journal of Soil and Water Conservation, 71, 61A–67A, https://doi.org/10.2489/jswc.71.3.61a, 2016.

Osterkamp, W. R., Hupp, C. R., and Stoffel, M.: The interactions between vegetation and erosion: new directions for research at the interface of ecology and geomorphology, Earth Surface Processes and Landforms, 37, 23–36, https://doi.org/10.1002/esp.2173, 2011.

Panagos, P., Meusburger, K., Ballabio, C., Borrelli, P., and Alewell, C.: Soil erodibility in Europe: A high-resolution dataset based on LUCAS, Science of The Total Environment, 479-480, 189–200, https://doi.org/10.1016/j.scitotenv.2014.02.010, 2014.

Panagos, P., Ballabio, C., Borrelli, P., Meusburger, K., Klik, A., Rousseva, S., Tadić, M. P., Michaelides, S., Hrabalíková, M., Olsen, P., Aalto, J., Lakatos, M., Rymszewicz, A., Dumitrescu, A., Beguería, S., and Alewell, C.: Rainfall erosivity in Europe, Science of The Total Environment, 511, 801–814, https://doi.org/10.1016/j.scitotenv.2015.01.008, 2015a.

Panagos, P., Borrelli, P., and Meusburger, K.: A New European Slope Length and Steepness Factor (LS-Factor) for Modeling Soil Erosion by Water, Geosciences, 5, 117–126, https://doi.org/10.3390/geosciences5020117, 2015b.

Panagos, P., Borrelli, P., Meusburger, K., Alewell, C., Lugato, E., and Montanarella, L.: Estimating the soil erosion cover-management factor at the European scale, Land Use Policy, 48, 38–50, https://doi.org/10.1016/j.landusepol.2015.05.021, 2015c.

Panagos, P., Borrelli, P., Meusburger, K., van der Zanden, E. H., Poesen, J., and Alewell, C.: Modelling the effect of support practices (P-factor) on the reduction of soil erosion by water at European scale, Environmental Science & Policy, 51, 23–34, https://doi.org/10.1016/j.envsci.2015.03.012, 2015d.

Panagos, P., Borrelli, P., Poesen, J., Ballabio, C., Lugato, E., Meusburger, K., Montanarella, L., and Alewell, C.: The new assessment of soil loss by water erosion in Europe, Environmental Science & Policy, 54, 438–447, https://doi.org/10.1016/j.envsci.2015.08.012, 2015e.

Panagos, P., Borrelli, P., Poesen, J., Meusburger, K., Ballabio, C., Lugato, E., Montanarella, L., and Alewell, C.: Reply to "The new assessment of soil loss by water erosion in Europe. Panagos P. et al., 2015 Environ. Sci. Policy 54, 438-447 - A response" by Evans and Boardman [Environ. Sci. Policy 58, 11-15], Environmental Science & Policy, 59, 53–57, https://doi.org/10.1016/j.envsci.2016.02.010, 2016.

Panagos, P., Ballabio, C., Meusburger, K., Spinoni, J., Alewell, C., and Borrelli, P.: Towards estimates of future rainfall erosivity in Europe based on REDES and WorldClim datasets, Journal of Hydrology, 548, 251–262, https://doi.org/10.1016/j.jhydrol.2017.03.006, 2017.

Panagos, P., Ballabio, C., Poesen, J., Lugato, E., Scarpa, S., Montanarella, L., and Borrelli, P.: A Soil Erosion Indicator for Supporting Agricultural, Environmental and Climate Policies in the European Union, Remote Sensing, 12, 1365, https://doi.org/10.3390/rs12091365, 2020.

Panagos, P., Ballabio, C., Himics, M., Scarpa, S., Matthews, F., Bogonos, M., Poesen, J., and Borrelli, P.: Projections of soil loss by water erosion in Europe by 2050, Environmental Science and Policy, 124, 380–392, https://doi.org/10.1016/j.envsci.2021.07.012, 2021.

Parton, W. J., Anderson, D. W., Cole, C. V., and Stewart, J. W. B.: Simulation of soil organic matter formation and mineralization in semiarid agroecosystems, in: Nutrient cycling in agricultural ecosystems, Special Publ. No. 23., The Univ. of Georgia, College of Agriculture Experiment Stations, 1983.

Parton, W. J., Stewart, J. W. B., and Cole, C. V.: Dynamics of C, N, P and S in grassland soils: a model, Biogeochemistry, 5, 109–131, https://doi.org/10.1007/bf02180320, 1988.

Pelletier, J., Broxton, P., Hazenberg, P., Zeng, X., Troch, P., et al.: Global 1-km Gridded Thickness of Soil, Regolith, and Sedimentary Deposit Layers, https://doi.org/10.3334/ORNLDAAC/1304, 2016.

Poggio, L., de Sousa, L. M., Batjes, N. H., Heuvelink, G. B. M., Kempen, B., et al.: SoilGrids 2.0: producing soil information for the globe with quantified spatial uncertainty, SOIL, 7, 217–240, https://doi.org/10.5194/soil-7-217-2021, 2021.

Powell, M. J. D.: The NEWUOA software for unconstrained optimization without derivatives, in: Nonconvex Optimization and Its Applications, pp. 255–297, Springer US, https://doi.org/10.1007/0-387-30065-1_16, 2006.

Powell, M. J. D.: Developments of NEWUOA for minimization without derivatives, IMA Journal of Numerical Analysis, 28, 649–664, https://doi.org/10.1093/imanum/drm047, 2008.

Quijano, L., Beguería, S., Gaspar, L., and Navas, A.: Estimating erosion rates using 137Cs measurements and WATEM/SEDEM in a Mediterranean cultivated field, CATENA, 138, 38–51, https://doi.org/10.1016/j.catena.2015.11.009, 2016.

Quine, T. A. and van Oost, K.: Insights into the future of soil erosion, Proceedings of the National Academy of Sciences, 117, 23 205–23 207, https://doi.org/10.1073/pnas.2017314117, 2020a.

Quine, T. A. and van Oost, K.: Insights into the future of soil erosion, Proceedings of the National Academy of Sciences, 117, 23 205–23 207, https://doi.org/10.1073/pnas.2017314117, 2020b.

Quinn, P., Beven, K., Chevallier, P., and Planchon, O.: The prediction of hillslope flow paths for distributed hydrological modelling using digital terrain models, Hydrological Processes, 5, 59–79, https://doi.org/10.1002/hyp.3360050106, 1991.

Renard, K.: Predicting soil erosion by water : a guide to conservation planning with the revised universal soil loss equation (RUSLE, U.S. Dept. of Agriculture, Agricultural Research Service For sale by the U.S. G.P.O., Supt. of Docs, Washington, D.C, 1997.

Renard, K. G., Foster, G. R., Weesies, G. A., and Porter, J. P.: RUSLE: Revised universal soil loss equation, Journal of Soil and Water Conservation, 46, 30–33, https://www.jswconline.org/content/46/1/30, 1991.

Robert, M.: Soil carbon sequestration for improved land management, Food and Agricultural Organization of the United Nations, Rome, 2001.

Roe, S., Streck, C., Obersteiner, M., Frank, S., Griscom, B., Drouet, L., Fricko, O., Gusti, M., Harris, N., Hasegawa, T., Hausfather, Z., Havlík, P., House, J., Nabuurs, G.-J., Popp, A., Sánchez, M. J. S., Sanderman, J., Smith, P., Stehfest, E., and Lawrence, D.: Contribution of the land sector to a 1.5 °C world, Nature Climate Change, 9, 817–828, https://doi.org/10.1038/s41558-019-0591-9, 2019.

Rompaey, A. J. J. V., Verstraeten, G., van Oost, K., Govers, G., and Poesen, J.: Modelling mean annual sediment yield using a distributed approach, Earth Surface Processes and Landforms, 26, 1221–1236, https://doi.org/10.1002/esp.275, 2001.

Rompaey, A. V., Bazzoffi, P., Jones, R. J., and Montanarella, L.: Modeling sediment yields in Italian catchments, Geomorphology, 65, 157–169, https://doi.org/10.1016/j.geomorph.2004.08.006, 2005.

Sanderman, J., Hengl, T., and Fiske, G. J.: Soil carbon debt of 12, 000 years of human land use, Proceedings of the National Academy of Sciences, 114, 9575–9580, https://doi.org/10.1073/pnas.1706103114, 2017.

Schewe, J., Gosling, S. N., Reyer, C., Zhao, F., Ciais, P., Elliott, J., Francois, L., Huber, V., Lotze, H. K., Seneviratne, S. I., van Vliet, M. T. H., Vautard, R., Wada, Y., Breuer, L., Büchner, M., Carozza, D. A., Chang, J., Coll, M., Deryng, D., de Wit, A., Eddy, T. D., Folberth, C., Frieler, K., Friend, A. D., Gerten, D., Gudmundsson, L., Hanasaki, N., Ito, A., Khabarov, N., Kim, H., Lawrence, P., Morfopoulos, C., Müller, C., Schmied, H. M., Orth, R., Ostberg, S., Pokhrel, Y., Pugh, T. A. M., Sakurai, G., Satoh, Y., Schmid, E., Stacke, T., Steenbeek, J., Steinkamp, J., Tang, Q., Tian, H., Tittensor, D. P., Volkholz, J., Wang, X., and Warszawski, L.: State-of-the-art global models underestimate impacts from climate extremes, Nature Communications, 10, https://doi.org/10.1038/s41467-019-08745-6, 2019.

Shangguan, W., Dai, Y., Duan, Q., Liu, B., and Yuan, H.: A global soil data set for earth system modeling, Journal of Advances in Modeling Earth Systems, 6, 249–263, https://doi.org/https://doi.org/10.1002/2013MS000293, 2014.

Sierra, C. A. and Müller, M.: A general mathematical framework for representing soil organic matter dynamics, Ecological Monographs, 85, 505–524, https://doi.org/10.1890/15-0361.1, 2015.

Sierra, C. A., Ceballos-Núñez, V., Metzler, H., and Müller, M.: Representing and Understanding the Carbon Cycle Using the Theory of Compartmental Dynamical Systems, Journal of Advances in Modeling Earth Systems, 10, 1729–1734, https://doi.org/10.1029/2018ms001360, 2018.

Soussana, J.-F., Lutfalla, S., Ehrhardt, F., Rosenstock, T., Lamanna, C., Havlík, P., Richards, M., Wollenberg, E. L., Chotte, J.-L., Torquebiau, E., Ciais, P., Smith, P., and Lal, R.: Matching policy and science: Rationale for the '4 per 1000 - soils for food security and climate' initiative, Soil and Tillage Research, 188, 3–15, https://doi.org/10.1016/j.still.2017.12.002, 2019.

Statistical Office of the European Union: Agriculture, forestry and fishery statistics: 2020 edition., European Commission, https://doi.org/10.2785/143455, 2020.

Strang, G.: Introduction to linear algebra, Cambridge Press, Wellesley, MA, 2016.

United Nations Environment Programme: GEMStat database of the Global Environment Monitoring System for Freshwater (GEMS/Water) Programme, https://gemstat.org/data/, accessed: 2021-11-15, 2018.

van Oost, K., Govers, G., Quine, T. A., Heckrath, G., Olesen, J. E., Gryze, S. D., and Merckx, R.: Landscape-scale modeling of carbon cycling under the impact of soil redistribution: The role of tillage erosion, Global Biogeochemical Cycles, 19, n/a–n/a, https://doi.org/10.1029/2005gb002471, 2005.

van Oost, K., Quine, T. A., Govers, G., Gryze, S. D., Six, J., Harden, J. W., Ritchie, J. C., McCarty, G. W., Heckrath, G., Kosmas, C., Giraldez, J. V., da Silva, J. R. M., and Merckx, R.: The Impact of Agricultural Soil Erosion on the Global Carbon Cycle, Science, 318, 626–629, https://doi.org/10.1126/science.1145724, 2007.

Wang, H. and Ranalli, M. G.: Low-Rank Smoothing Splines on Complicated Domains, Biometrics, 63, 209–217, https://doi.org/10.1111/j.1541-0420.2006.00674.x, 2006.

Wang, Z., Doetterl, S., Vanclooster, M., van Wesemael, B., and van Oost, K.: Constraining a coupled erosion and soil organic carbon model using hillslope-scale patterns of carbon stocks and pool composition, Journal of Geophysical Research: Biogeosciences, 120, 452–465, https://doi.org/10.1002/2014jg002768, 2015.

Wang, Z., Hoffmann, T., Six, J., Kaplan, J. O., Govers, G., Doetterl, S., and van Oost, K.: Human-induced erosion has offset one-third of carbon emissions from land cover change, Nature Climate Change, 7, 345–349, https://doi.org/10.1038/nclimate3263, 2017.

Washington, W. M., Buja, L., and Craig, A.: The computational future for climate and Earth system models: on the path to petaflop and beyond, Philosophical Transactions of the Royal Society A: Mathematical, Physical and Engineering Sciences, 367, 833–846, https://doi.org/10.1098/rsta.2008.0219, 2008.

Wischmeier, W., Smith, D., Science, U. S., Administration, E., and Station, P. U. A. E.: Predicting Rainfall Erosion Losses: A Guide to Conservation Planning, Agriculture handbook, Department of Agriculture, Science and Education Administration, 1978.

Wood, S. N.: Low-Rank Scale-Invariant Tensor Product Smooths for Generalized Additive Mixed Models, Biometrics, 62, 1025–1036, https://doi.org/10.1111/j.1541-0420.2006.00574.x, 2006.

Xia, J. Y., Luo, Y. Q., Wang, Y.-P., Weng, E. S., and Hararuk, O.: A semi-analytical solution to accelerate spin-up of a coupled carbon and nitrogen land model to steady state, Geoscientific Model Development, 5, 1259–1271, https://doi.org/10.5194/gmd-5-1259-2012, 2012.